A PMSG-BASED WIND ENERGY CONVERSION SYSTEM ASSISTED BY PHOTOVOLTAIC POWER

A Thesis
Submitted to the Graduate Faculty
of the
North Dakota State University
of Agriculture and Applied Science

By

Abrez Mondal

In Partial Fulfillment
for the Degree of
MASTER OF SCIENCE

Major Department:
Electrical and Computer Engineering

May 2012

Fargo, North Dakota

North Dakota State University
Graduate School

Title

A PMSG-BASED WIND ENERGY CONVERSION SYSTEM ASSISTED BY

PHOTOVOLTAIC POWER

By

Abrez Mondal

The Supervisory Committee certifies that this ***disquisition*** complies with North Dakota State University's regulations and meets the accepted standards for the degree of

MASTER OF SCIENCE

SUPERVISORY COMMITTEE:

Subbaraya Yuvarajan
Chair

Rajesh Kavasseri

Cristinel Ababei

Sanku Mallik

Approved:

05/21/2012
Date

Rajendra Katti
Department Chair

ABSTRACT

This work discusses a hybrid power conversion scheme consisting of a permanent magnet synchronous generator (PMSG)-based wind energy system and photovoltaic panels. The two energy sources are integrated with a battery to store extra photovoltaic energy during the day and to meet any additional power requirement in the absence of sunlight. The PV panel is interfaced to the battery through a SEPIC converter for maximum power point tracking. The wind energy from the PMSG is supplied to the battery through a boost converter which regulates the output. The total power obtained from the hybrid system is fed to a three-phase load through an inverter implementing Space-vector pulse-width modulation. The controller modeled in MATLAB/Simulink software is simple and is implemented through real time simulation using dSPACE hardware.

ACKNOWLEDGEMENTS

I am grateful to my advisor Dr. Subbaraya Yuvarajan for his support, patience and guidance in completing this research work. He always provided me the necessary background required for conducting this research work and without his help I would have not been able to complete my research.

I would also like to thank Dr. Rajesh Kavasseri, Dr. Cristinel Ababei and Dr. Sanku Mallik for their time and support as members of my graduate committee. I am also thankful to the Department of Electrical and Computer Engineering and the Graduate School at North Dakota State University for providing me with financial support for completing my graduate study.

Finally, I am deeply indebted to my beloved parents for their constant love and encouragement.

TABLE OF CONTENTS

LIST OF TABLES

LIST OF FIGURES

CHAPTER 1. INTRODUCION

The depletion in the reserves of fossil fuels, considered as traditional sources of power generation, at an alarming rate coupled with the level of environmental pollution associated with them have shifted the focus towards harvesting non-conventional energy sources such as wind and solar energy for power generation. The thesis work proposes a hybrid renewable energy conversion scheme using both wind and photovoltaic energy sources.

1.1 Wind Energy Systems

Wind energy conversion systems convert the kinetic energy associated with wind speed into electrical energy for feeding power to the grid. The energy is captured by the blades of wind turbines whose rotor is connected to the shaft of electric generators. The wind power rotates the turbine blades which in turn drive the electric generators resulting in the generation of electric power at the output of the machine. The power output from such wind energy conversion systems depend on the wind speed and the pitch angle of the turbine blades. The wind energy conversion systems (WECSs) initially used squirrel-cage induction machines for fixed speed operation. Later, variable speed wind energy systems emerged and doubly fed induction generators (DFIGs) were used increasingly. The wind generation systems using permanent magnet synchronous generators (PMSGs) represent a further advancement in this area [1]. Variable speed wind energy systems are particularly suitable for extracting maximum power from wind energy and are more efficient than fixed speed systems. Several maximum power point tracking schemes are implemented to harness the total energy from wind at various wind speeds and blade pitch angle values [2]. However, for low speed systems typically using PMSGs, pitch angle control is rarely used. The power extracted from wind needs to be fed to the AC grid. Several power electronic converters are

employed to achieve this goal and they considerably improve the power quality before feeding the power to the grid. The grid-side converters (inverters) play an important role in meeting the strict voltage and frequency requirements of AC grid.

1.2 Photovoltaic Systems

Solar or photovoltaic (PV) energy has gained increased attention as a prominent renewable energy source. The progress made in semiconductor technology has helped immensely in designing efficient solar panels which are used in power applications. Solar energy is considered as one of the primary renewable energy sources because it is abundant, pollution free and recyclable but the high initial costs involved in the installation of PV systems has so far hindered its extensive usage. Moreover, the non-linear characteristics of the PV panels call for implementing complex control algorithms. The electrical power derived from PV panels is greatly affected by the prevailing atmospheric conditions such as temperature and illumination level. The maximum power (MPP) obtained from a PV panel increases with insolation and decreases with ambient temperature. Many harvesting schemes use microcontrollers or digital signal processors for maximum power point tracking (MPPT) based on a perturbation and observation (P&O) technique [3], [4]. But the main disadvantage of the P&O approach is that it leads to lot of oscillations. Some approximate methods also exist which use the linearity between current at MPP and the short-circuit current [5], [6]. There are also MPPT schemes which are improved versions of P&O approach and those using frequency-injection techniques [7]-[9].

1.3 Scope of Work

The thesis work presents a hybrid scheme for conversion of energy from two non-conventional sources of power. The energy conversion system integrates both wind and

photovoltaic energy sources, thereby making the system more reliable and efficient. The system developed in this work is a standalone one and is useful for generating power in remote areas. The wind energy subsystem uses a permanent magnet synchronous generator for energy conversion and is useful for operation under varying conditions. The PV subsystem uses maximum power point tracking technique in order to maximize the photovoltaic power output. A battery is used as a storage unit in this system and it also supplies additional power during the night when sunlight is unavailable. A single voltage source inverter is used for obtaining a three-phase AC voltage output. The commonly used switching scheme for three-phase inverters is the sinusoidal pulse-width modulation but it does not take advantage of the three-phase properties of voltages. In this work, the inverter uses space-vector pulse-width modulation technique for generating the switching signals and thus results in a higher output voltage level and a lower value for total harmonic distortion. The most salient feature of this work is that the entire system is operated using computer-based control and does not have any physical controllers in hardware and makes the system more flexible. The controller is modeled using MATLAB/Simulink software and is connected to the real system (plant) using dSPACE hardware.

1.4 Contributions

The thesis work proposes a hybrid power conversion scheme harnessing both wind and solar energy sources. The wind energy conversion system uses a permanent magnet synchronous machine as the electric generator while the photovoltaic system implements a maximum power point tracking scheme. Unlike the MPPT schemes referred in the previous sections, the proposed method uses the exact equations of the PV panel so it is fast and accurate. A novel method of integrating both the wind generator and the photovoltaic panel

using a single DC link has been presented. A battery connected at the DC link serves as the storage unit. The two energy sources aid each other in supplying load demand and also the battery serves as a back-up unit. Furthermore, this configuration requires a single inverter for AC conversion instead of two separate inverters that are used in other hybrid renewable energy systems where the wind and PV units supply the load separately as two independent units. The entire system has been implemented in hardware with a single DSP-based controller unit using MATLAB-Simulink and dSPACE.

1.5 Outline of Thesis

Chapter 2 introduces the design tools used for computer based control. The process of implementing a DSP-based control scheme using rapid-prototyping tool is discussed in detail. The method of real-time implementation of a software based controller and its communication with the physical hardware is elaborated.

Chapter 3 presents the different renewable energy sources used in this work, namely wind and photovoltaic energy. General wind energy conversion systems are briefly discussed. Also, the different maximum power point tracking schemes commonly used for maximizing photovoltaic energy are reviewed.

Chapter 4 mainly concentrates on the different power electronic converters used for the thesis work such as rectifiers, DC-DC converters and inverters. The chapter explains the topology selection for the DC-DC converters and also presents a comparison between the different pulse-width modulation techniques used for inverters.

Chapter 5 reviews the different components of wind energy conversion systems such as wind turbines and electric generators. Since this work uses a permanent magnet synchronous

machine for generating electric power, the characteristics and the structure of such machines are discussed in detail.

Chapter 6 shows the mathematical derivation of the maximum power point tracking algorithm followed in this work for the photovoltaic system. Also, its implementation using dSPACE and Simulink and the practical results obtained are presented. Chapter 7 mainly gives the results obtained through hardware implementation of the hybrid scheme. Finally, Chapter 8 summarizes the work done in this thesis and also lists some suggestions for future research work.

CHAPTER 2. DESIGN TOOLS FOR RENEWABLE ENERGY CONVERSION

2.1 Introduction

The thesis work involves the design of a hybrid renewable energy conversion system. In order to make the complete system operate under optimal conditions, several controllers for power converter stages need to be designed. In this work, a computer-based control approach has been implemented using MATLAB-Simulink modeling tool and dSPACE hardware and thus warrants a discussion about the development tools used.

2.2 DSP-based Control Scheme

The DSP-based controller has two major components for the hardware and software, namely i) DS 1104 R&D Controller card and CP 1104 I/O board and ii) MATLAB/Simulink and Control-desk. The details of the components are presented in this section.

2.2.1 DS 1104 R&D controller card and CP 1104 I/O board

dSPACE is a rapid-prototyping tool which helps to create and test control algorithms developed in MATLAB/Simulink and implement them in actual hardware set-up. The dSPACE system in conjunction with MATLAB/Simulink forms a hardware-in-the-loop (HIL) simulation arrangement and is useful for real-time implementation. The DS 1104 R&D Controller card and CP 1104 I/O board constitutes the hardware components of the dSPACE system. The DS 1104 R&D Controller card is plugged into a PCI slot of a computer. The DS 1104 is a high-speed digital controller used for real-time simulations. The system is based on a 603 PowerPC floating-point processor running at 250 MHz and for advanced I/O purposes, a slave-DSP subsystem based on TMS320F240 DSP microcontroller is used [10]. The DSP controller (DS 1104 R&D Controller card) generates control action in discrete time-steps. The nature of the control action is governed by the type of programming done for this

controller card using the real-time interface of MATLAB/Simulink. Real feedback signals (voltage, current, generator speed etc.) from the plant under control are fed to the controller through the input ports of the CP 1104 I/O board. Based on the feedback inputs, digital signals are generated following the algorithm developed in MATLAB Simulink and fed to the external plant.

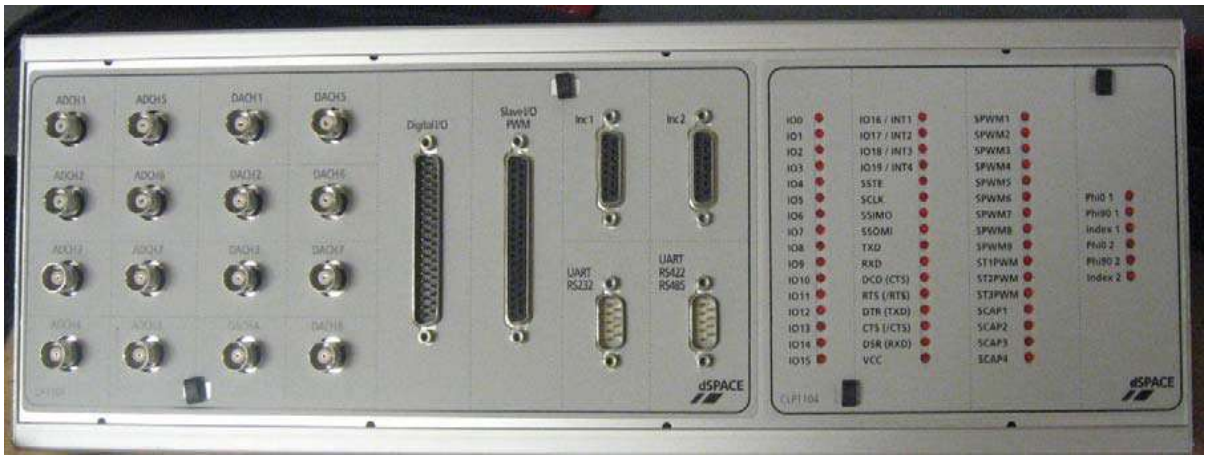

Figure 2-1: CP 1104 I/O board

The CP 1104 I/O board acts as an interface for communicating with the external hardware set-up in the laboratory. Figure 2-1 shows a panel overview of the CP 1104 I/O board. There are 22 interfaces on the board. The first 16 ports are used for communication with the analog world through BNC connectors. Eight BNC connectors (ADCH1 to ADCH8) serve as input ports and are basically inputs of ADC channels. There are two types of ADC input channels on the CP 1104 I/O board namely, (i) one 16-bit ADC with four multiplexed input signals (ADCH1 to ADCH4) and (ii)four 12-bit parallel ADCs with one input signal (ADCH5 to ADCH8). The remaining 8 BNC connectors serve as analog outputs and are parallel DAC channels (DACH1 to DACH8). In addition, a bit I/O unit having 20 digital I/O pins is present. For high speed I/O operations, a slave DSP digital I/O having 37 pins is

present and are mostly used for high frequency PWM controls. There are two interfaces (Inc1 and Inc2) for incremental encoders and are used for tracking the speeds of rotating electrical machines. The CP 1104 I/O board also has options to communicate with external devices through two Universal Asynchronous Receiver and Transmitter (UART). Each UART can be configured as a RS232, RS422 or RS485 transceiver.

2.2.2 MATLAB/Simulink and Control-desk

Simulink is a commercial tool developed by Mathworks Inc. [11]. It operates in the MATLAB environment and is a simulation platform for model-based design of dynamic systems. When a control model is developed in Simulink, it needs to be tested on a real system and that necessitates the integration of the controller simulated in real time to the actual plant. This feature is called 'rapid control prototyping' and the simulation time of the model needs to match the time requirement of the real physical system. Real-Time Interface (RTI) acts as a linking medium which automatically generates the real-time C source code of Simulink models with the help of Simulink Coder (formerly known as Real-Time Workshop) and implements this code on the dSPACE real-time hardware [12]. The simulated controller is thus able to control the actual plant and this technique is referred to as hardware-in-the-loop (HIL) simulation. For HIL, real time simulation is of utmost importance and the simulated model must have enough computational power to carry out operations meeting the time constraints of real systems. The I/O ports of CP 1104 board are accessible from inside the Simulink library and the required dSPACE blocks have to be added in the Simulink model in order to connect the plant to the required I/O ports. When the Simulink control model is build (CTRL+B), the real-time option (RTI) implements the whole system inside the DSP of DS 1104. The controller in software (Simulink) gets converted to a real-time

system on hardware (DS 1104) [refXX]. Simulink generates a System Description File (*.sdf) when the model is built (CTRL+B) and this file gives access to the different variables of the controller to a separate software called dSPACE Control-desk [13]. In this software, a control panel can be created which serves as a graphic use interface (GUI) for the system. Once the *.sdf file generated from Simulink is loaded into the Control-desk, the different variables of the controller can be linked to graphical instruments on layouts (*.lay file). The variables of the controller can thus be changed and monitored in real-time using the graphical instruments of Control-desk. The Control Desk provides bidirectional communication in real-time between the control panel and DS 1104. Figure 2-2 illustrates the functioning of a complete control system for PV panel using Simulink and dSPACE.

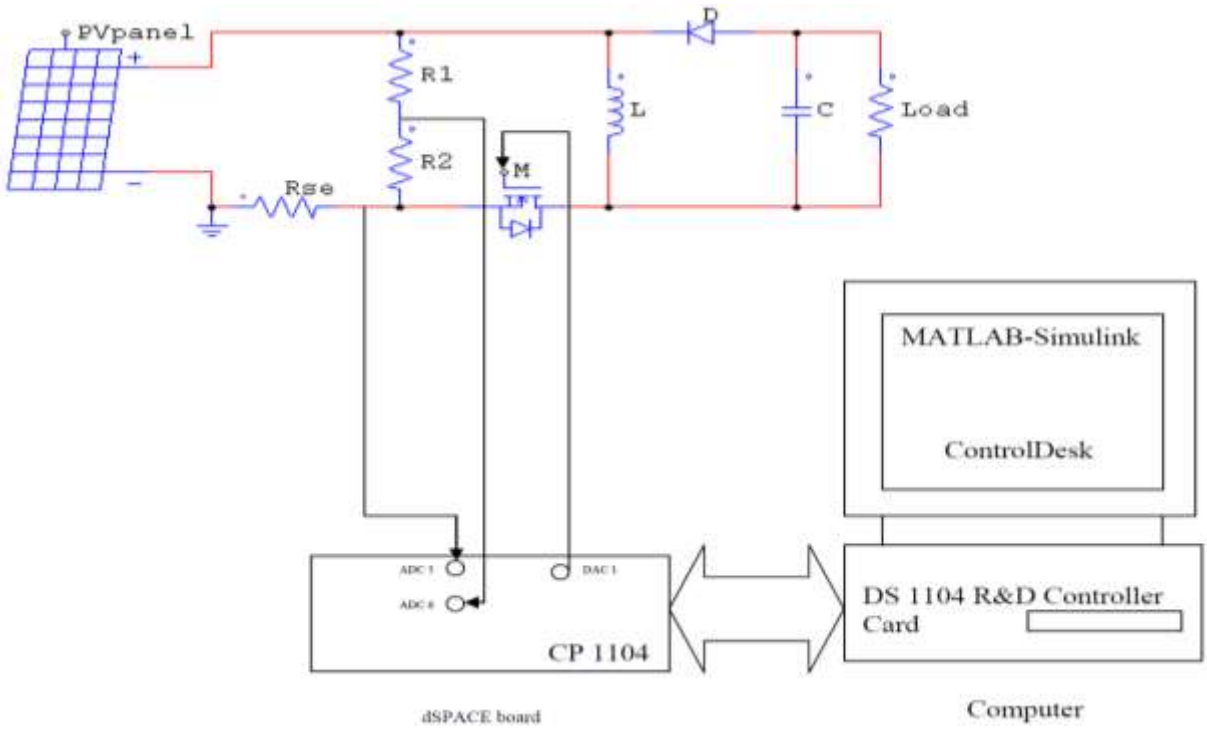

Figure 2-2: DSP based control using Simulink and dSPACE

2.3 Conclusions

In this chapter, a complete description of the design tools for developing the controller used in the thesis work has been provided. The procedure for building a control system in software (using Simulink) and thereby linking it to a hardware set-up (DS 1104) for connecting to the actual plant has been elaborated.

CHAPTER 3. REVIEW OF WIND AND SOLAR ENERGY SYSTEMS AND THEIR CHARACTERISTICS

3.1 Introduction to Renewable Energy Systems

Renewable energy sources have gained much prominence for power generation because the traditional energy sources such as coal, petroleum and natural gas are getting depleted at an alarming rate. Moreover, the conventional energy sources are becoming expensive and also add to the pollution level due to the emission of greenhouse gases during energy conversion. These factors have collectively shifted the focus towards harvesting the non-conventional sources of energy. Wind and solar energy are considered important renewable energy source owing to their abundance and clean form [14]. The work done in this thesis explores both the possibilities of wind and solar energy conversion.

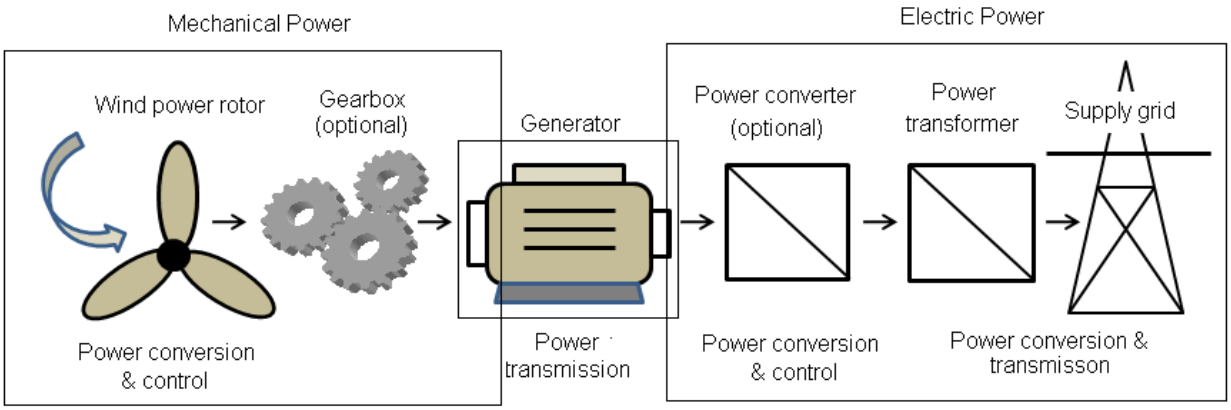

Figure 3-1: Wind Energy Conversion System

3.2 Wind Power Conversion

3.2.1 Introduction to wind energy conversion systems (WECS)

Wind energy is one of the cheapest forms of electric power generation and is environment friendly. These factors have contributed to the steady rise in the development of

wind energy conversion systems (WECS). A typical wind power conversion system is illustrated in Figure 3-1 and it consists of the turbine rotor, gearbox, generator, transformer and power converter stages.

3.2.2 Current wind turbine technology

Wind turbine systems are broadly classified into fixed-speed and variable-speed systems [15]. These two systems have been briefly discussed in this section.

3.2.2.1 Fixed-speed turbine systems

The early wind turbines that were installed were intended for operation at a particular speed [16]. Squirrel-cage induction machines are generally used as the generator and they are directly connected to the grid. Thus the grid frequency determines the speed of the generator and the turbine rotor as well. This type of system is called a single-speed WECS and is shown in Figure 3-2. A soft-starter is used to limit the high in-rush current (nearly 6 to 7

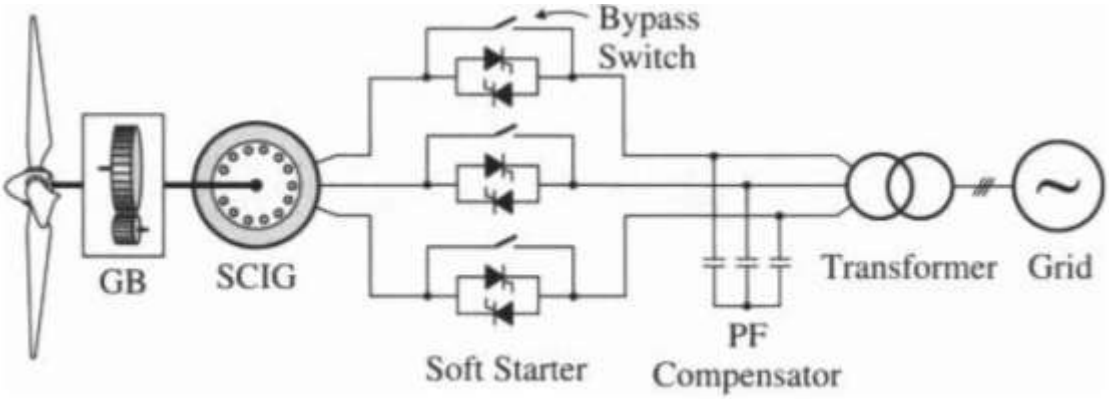

Figure 3-2: Fixed-Speed Wind Turbine System

times the rated current for a squirrel-cage induction machine) during starting. Also, an induction generator draws reactive power from the grid and in order to compensate the reactive power to support the voltage level, PF compensator is used. Another type of fixed-

speed system exists called the two-speed WECS. This system has a better energy conversion efficiency compared to the single-speed WECS and is achieved by pole-changing technique for the induction generator and also by having two separate generators mechanically coupled to a single shaft.

The advantage of a fixed-speed wind turbine system is that it is simple and cheaper to implement. But it requires a stiff grid condition to operate and since it is designed for fixed speed operations, the generator needs to be mechanically strong in order to absorb high mechanical stress due to strong wind gusts which cause torque pulsations and fluctuations in electrical power output.

3.2.2.2 Variable-speed turbine systems

The variable-speed wind turbine systems are commonly used for harnessing wind power. The variable-speed operation is realized by connecting an external resistance to a wound rotor induction generator or by a doubly-fed induction generator (DFIG) with an additional power converter feeding the rotor circuit. The systems using induction generators require an additional gearbox arrangement and are termed as indirect drive systems. Direct drive systems are also used for variable-speed operations and they do not need any additional gearbox. Direct drive operation is achieved by employing wound rotor synchronous generators with an additional magnetizing circuit for the rotor or by using a permanent magnet synchronous generator (PMSG). All generators are connected to the grid through power converters which control generator speed and also help to obtain a better output at the grid. Details about power converters will be discussed in Chapter 4. A variable-speed WECS using a synchronous generator is shown in Figure 3-3.

The power converters helps to control generator speed and so the variable-speed turbine systems are generally designed to obtain a better efficiency by tracking the maximum power point (MPP) of the wind turbines over a wide range of speeds. The maximum power point tracking methods are based on fuzzy logic based control [17] and sliding mode control [18].

The advantage of a variable-speed wind turbine system over its fixed-speed counterpart lies in its overall higher efficiency by extracting the maximum power possible. Also, the generators are not subjected to mechanical stresses due to wind gusts and results in a better

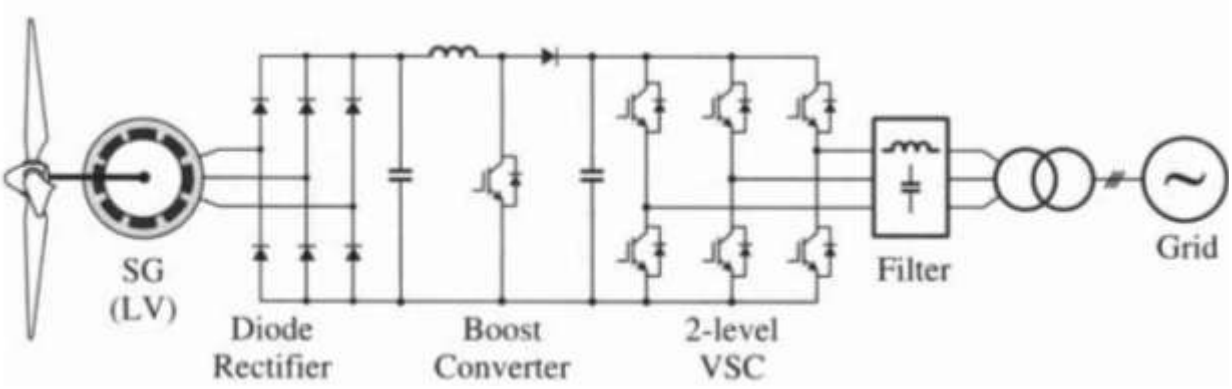

Figure 3-3: Variable-Speed Wind Turbine System

output performance. But the disadvantage of the variable-speed wind turbine system is that it requires additional power converters and complex control circuits. Also, the power electronic switches contribute towards switching power losses.

3.3 Photovoltaic Power

3.3.1 Introduction to PV systems

Solar or photovoltaic (PV) energy has gained increased attention as a prominent renewable energy source. A single converter cell is called a solar or photovoltaic cell and the power output of an individual cell is very small. Several PV cells are generally combined in series or parallel arrangement to form an array in order to increase the total power output. The

progress made in semiconductor technology has helped immensely in designing efficient photovoltaic panels which are used in power applications. Solar energy is considered as one of the primary renewable energy sources because it is abundant, pollution free and recyclable but the high initial costs involved in the installation of PV systems has so far hindered its extensive usage. Moreover, the non-linear characteristics of the PV panels call for implementing complex control algorithms.

3.3.2 PV panel characteristics

The current-voltage (I-V) characteristic of a PV panel is non-linear in nature and is given by [19]:

$$I = I_{sc} - I_{sat}[\exp\left(\frac{qV_{oc}}{AKT}\right) - 1] \quad (3.1)$$

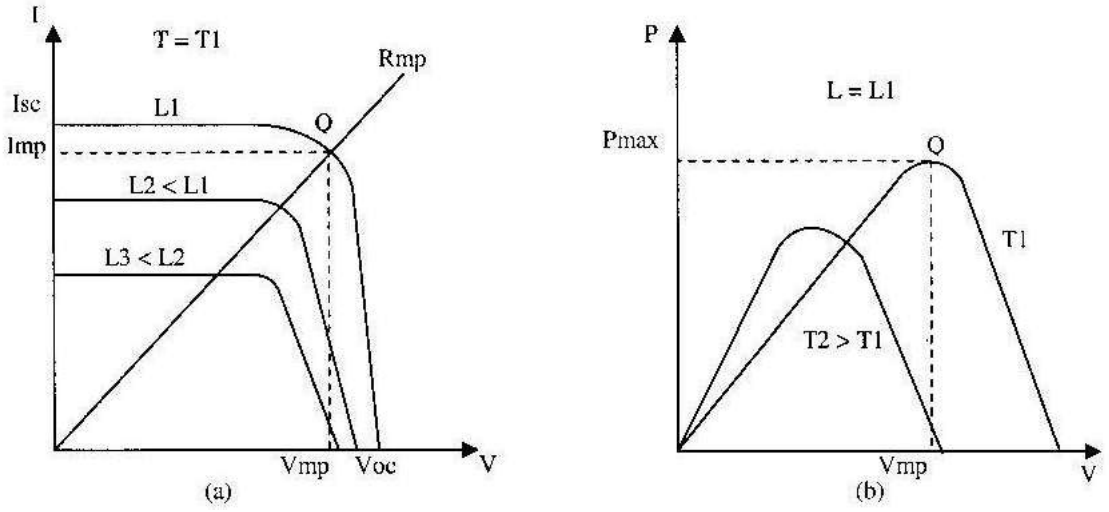

Figure 3-4: Characteristics of a PV Panel (a) I-V and (b) P-V Characteristics at different insolation level (L) and ambient temperature (T)

The electrical power derived from PV panels is greatly affected by the prevailing atmospheric conditions such as temperature and illumination level. The variations of the output current and output power of a PV panel as functions of output voltage for different insolation levels and temperature are shown in Figure 3-4. The maximum power is achieved only at a particular operating point Q called the maximum power point (MPP) of the panel. The maximum power obtained from a particular panel increases with the insolation and decreases with ambient temperature.

3.4 Maximum Power Point Tracking (MPPT) Schemes for PV Panels

Numerous maximum power point tracking (MPPT) schemes have been reported in literature [20]. But these techniques can be classified into four major categories namely, Perturb and Observe method, Incremental Conductance method, Fractional Open-circuit Voltage method and fractional Short-circuit Current method. These four methods have been elaborately discussed in this section.

3.4.1 Perturb and observe (P&O) method

Many harvesting schemes use microcontrollers or digital signal processors for maximum power point tracking (MPPT) based on a perturbation and observation (P&O) technique [3]. Figure 3-4(b) shows that an increase in the output voltage increases the output power while operating in the region left of the MPP. So, in the P&O method, the power measured at a particular sampling instant is compared with the value obtained during the previous sampling and if the perturbation in the duty cycle produced an increase in power the subsequent perturbation is kept in the same direction until the MPP is reached. Although this scheme is

easy to implement, the main disadvantage of the P&O approach is that it leads to lot of oscillations.

3.4.2 Incremental conductance method

The slope of the PV power curve (Fig. 3-4 (b)) is positive to the right of MPP, zero at MPP and negative to the left of MPP [21]. So, the following relationship can be derived at MPP

$$\frac{\Delta I}{\Delta V} = -\frac{I}{V}. \tag{3.2}$$

In this method, MPP is tracked by comparing the instantaneous conductance (I/V) to the incremental conductance (ΔI/ΔV). This method can track the MPP under rapidly changing atmospheric conditions but the main drawback is that it needs a complex control circuit.

3.4.3 Fractional open-circuit voltage method

This is an approximate method based on the near-linear relationship between the output voltage of the PV panel at MPP (V_{MPP}) and the open-circuit voltage of the PV panel (V_{OC}). This relationship is given by [22]

$$K_v = \frac{V_{MPP}}{V_{OC}}. \tag{3.3}$$

The proportionality constant,K_v, is approximately equal to 0.7 and is determined by the photovoltaic cell fabrication technology and weather conditions. In this method, the power converter is momentarily shut down at every sampling instant in order to measure $V_{OC}$and the control algorithm computes V_{MPP}following equation (3.3). The switching of the power converter is then carried out in a manner so as to match the operating voltage to the newly determined value of V_{MPP}. The implementation of this method is simple but the main

drawback is that the value of K_v is assumed constant even though it changes due to prevalent weather conditions and thus the MPP is not tracked correctly. Another disadvantage is that the power converter is shut down during every sampling instant leading to a reduced output power.

3.4.4 Fractional short-circuit current method

This is also an approximate method based on the near-linear relationship between the PV panel current at MPP (I_{MPP}) and the short-circuit current of the PV panel (I_{SC}). This relationship is given by [23]

$$K_i = \frac{I_{MPP}}{I_{SC}}. \tag{3.4}$$

The proportionality constant,K_i, is roughly equal to 0.9 and is dependent on the photovoltaic cell fabrication technology and weather conditions. In this method, the switch in the power converter is triggered with a relatively long pulse once in every sampling interval in order to measure I_{SC} and the control algorithm computes I_{MPP} following equation (3.3). The switching of the power converter is then carried out in a manner so as to match the panel current to the newly determined value of I_{MPP}. The main drawback of this method is that the value of K_i is assumed constant even though it changes due to prevalent weather conditions and thus the scheme is not a true MPP tracker. Another disadvantage is that the photovoltaic power is unavailable once in every sampling interval for I_{SC} measurements.

3.4.5 MPPT scheme based on PV panel equations

This work implements an MPPT scheme which is derived based on the open-circuit voltage and the short-circuit current of a PV panel. Detailed mathematical derivation of this

equation is presented and the Simulink model for the control scheme is shown in Chapter 6. The power circuit involves a pulse-width modulated (PWM) DC-DC converter between the PV panel and the load. The MPPT is realized by sensing the short-circuit current and the open-circuit voltage and adjusting the duty-cycle of the DC-DC converter and hence the converter output current such that the MPPT equation holds. The proposed method focuses on the delivery of maximum power under all environmental conditions and eliminates complex control circuitry for the MPP tracker resulting in an efficient and inexpensive PV system.

3.5 Conclusions

This chapter introduced two important renewable energy sources namely, wind and solar energy and stresses about their importance in power generation. The different wind energy conversion systems were discussed in detail and their advantages and disadvantages were presented. Next, the characteristics of photovoltaic panels were illustrated and some of the schemes for extracting the maximum power from the PV panels were discussed in detail and the advantages and disadvantages of each method were listed.

CHAPTER 4. POWER ELECTRONIC CONVERTERS FOR RENEWABLE ENERGY SYSTEMS

4.1 Introduction

The advent of power electronics have greatly contributed to the reliability of existing power networks. The renewable energy systems are no exception. The power electronic converters play an important role in obtaining a better power quality at the output. They also help in extracting the maximum possible power from renewable energy sources following maximum power point tracking algorithms. In this work, the power converters used are diode rectifiers, DC-DC converters for achieving desired DC voltage levels, and inverters for obtaining an AC output from DC.

The variable-frequency output voltage from the PMSG is finally converted into a sinusoidal ac voltage at grid frequency before being fed to the grid. In order to achieve this conversion, power electronic converters are used. Two general topologies adopted are (a) a diode rectifier followed by a boost converter and an inverter and (b) back-to-back converter system [24]. In the first scheme, the switching signal for the boost converter is generated following some control algorithm and the inverter switching is done using pulse width modulation technique. This work develops a wind energy conversion system with a PMSG using a diode rectifier, a DC-DC converter and an inverter using space vector pulse width modulation (SVPWM) [25]. The PV system uses a DC-DC converter and the necessary switching signal following proper voltage and power matching conditions [26].

4.2 Diode Rectifier

The diode rectifier is used in this work for converting the three-phase output AC voltage at the terminals of the PMSG into a DC voltage. The rectified output dc voltage (V_{rec}) from a

three-phase diode rectifier is given by [27]

$$V_{rec} = \frac{3\sqrt{2}}{\pi} V_{llrms} \tag{4.1}$$

where $V_{llrms}$is the rms value of the line-to-line voltage applied to the rectifier.

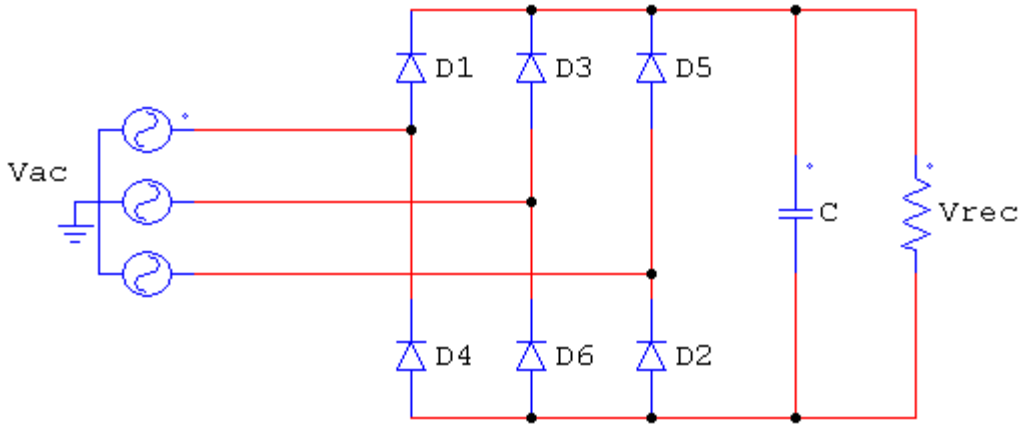

Figure 4-1: Three-phase diode rectifier

The circuit diagram for a three-phase diode rectifier is shown in Figure 4-1. The rectified output from the diode rectifier is uncontrolled but it does not have any additional losses owing to the switching of any power electronic components. It can, therefore, be assumed that the total power obtained from PMSG is converted from AC to DC if the diode losses are negligible.

4.3 DC-DC Converters

The DC-DC converters are generally used to obtain an average output voltage above or below the input voltage. In this work, the DC-DC converters are used as interfacing units in order to obtain a matching voltage from both the wind and photovoltaic systems. Depending on the output voltage level, the three most commonly used topologies are buck, boost and buck-boost converters. The components involved in each of the three converters are the same

and only the arrangement of those components in the circuit causes the variation in the nature input-output relation. Each of the three topologies is discussed in detail in this section.

4.3.1 Buck converter

The voltage obtained at the output (V_o) of a buck converter is lower than that at its input terminals (V_{in}) and is given for continuous inductor current by [27]

$$V_o = dV_{in} \tag{4.2}$$

where *d* is the duty cycle for the switch. The circuit diagram for a buck converter is shown in Figure 4-2. The switch is connected directly to the input terminal and so the input current becomes discontinuous.

4.3.2 Boost converter

The circuit diagram for a boost converter is shown in Figure 4-3. The voltage obtained at the output (V_o) of a buck converter is higher than that at its input terminals (V_{in}) and under continuous current mode (CCM) of operation is given by [27]

$$V_o = \frac{V_{in}}{1-d} \tag{4.3}$$

where *d* is the duty cycle for the switch.

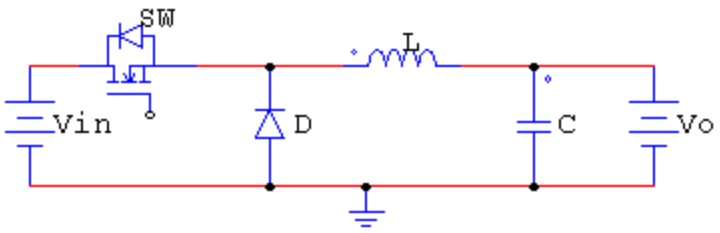

Figure 4-2: Buck converter

The boost converter requires a larger inductor (L) and output filter capacitor (C) as compared to the buck converter but the input current can be kept continuous by properly choosing the inductor and capacitor.

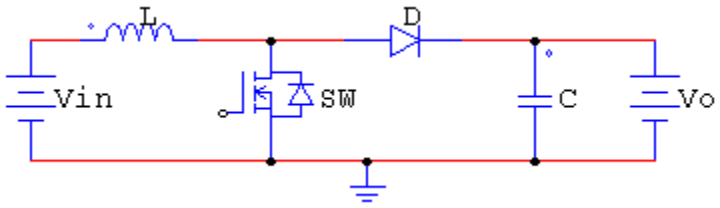

Figure 4-3: Boost converter

4.3.3 Buck-boost converter

The output voltage of a buck-boost converter (V_o) can be higher or lower than its input voltage (V_{in}) depending on the choice of the duty cycle *d*. The circuit of a buck-boost converter is shown in Figure 4-4. The steady state output voltage under continuous current mode (CCM) of operation is given by [27]

$$V_o = \frac{-dV_{in}}{1-d}\,. \tag{4.4}$$

The polarity of the output voltage is opposite to that of the input. The switch is connected directly to the input terminal which makes the input current discontinuous.

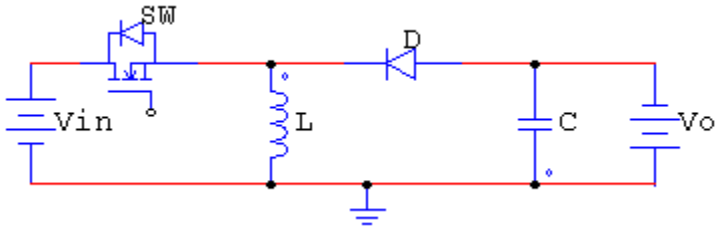

Figure 4-4: Buck-boost converter

4.3.4 SEPIC converter

Single-ended primary-inductor converter (SEPIC) is a DC-DC converter where its output voltage (V_o) can be greater, less or equal to its input voltage (V_{in}) and can be controlled by varying the duty cycle *d* of the primary transistor switch. It is similar to a traditional buck-boost converter but has the advantage of a non-inverted output voltage. But on the downside, the components used are more and the analysis of its operation is more complex. The output current in SEPIC is pulsating while its input current can be made continuous by proper choice of its primary inductor (L_1). The circuit diagram for a SEPIC has been shown in Figure 4.5. The steady state output voltage under continuous current mode (CCM) of operation is given by [28]:

$$V_o = \frac{dV_{in}}{1-d} . \tag{4.5}$$

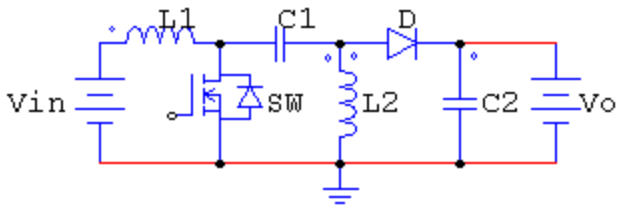

Figure 4-5: SEPIC converter

4.4 Inverters

Inverters are basically power electronic converters used for converting a DC input voltage to an AC output at a particular frequency. In this work, a three-phase voltage source inverter (VSI) is used to convert the dc link voltage obtained at the output of a DC-DC converter to a three-phase AC voltage so that it can be fed to an AC load. Figure 4-6 shows the schematic diagram of a three-phase voltage source inverter circuit. The switches used are

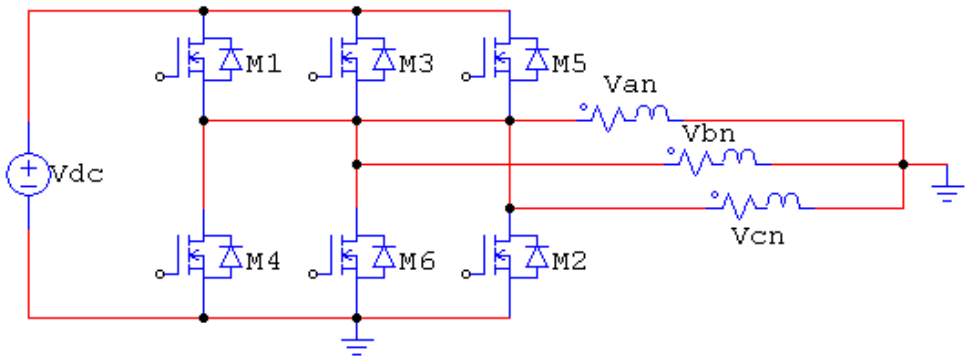

Figure 4-6: Three-phase inverter

usually MOSFETs or IGBTs and their switching signals are generally obtained using a suitable Pulse-width Modulation (PWM) technique.

4.4.1 Sine PWM inverters

The pulse-width modulation (PWM) schemes are very efficient for the voltage control of three-phase inverters. The output voltage magnitude and its frequency can be controlled by using different PWM schemes. The sine PWM (SPWM) control strategy is one of the most commonly used methods for the control of voltage source inverters. In the SPWM scheme, three reference sinusoidal waveforms (v_{ar}, v_{br} and v_{cr}) known as the modulating waveforms are compared with a higher frequency triangular wave called the carrier signal (v_{tr}). The three reference sinusoidal waveforms correspond to the three phases of the inverter and have equal amplitude and are 120° out of phase with respect to each other. The frequency of the reference sinusoidal signals determines the fundamental output frequency (f_o) of the inverter. The amplitude (V_m) of the reference sine waves controls the amplitude modulation ratio (m_a) defined as [29]

$$m_a = \frac{V_m}{V_{tr}} \tag{4.6}$$

where V_m and V_{tr} are the peak values of the reference and carrier signals respectively.

The magnitude of the inverter output voltage is dependent on the amplitude modulation index. The value of m_a is normally adjusted by varying the peak value of the modulating signal while keeping the carrier triangular wave signal fixed.

The frequency modulation index (m_f) is defined as

$$m_f = \frac{f_c}{f_r} \tag{4.7}$$

where f_c and f_r are the frequencies of the reference and carrier signals respectively.
The value of m_f is chosen to be an odd multiple of 3. The phase voltages at the output are displaced by 120°. The line-to-line output voltages are symmetric and are devoid of any even harmonics. In the line-to-line voltage waveform, the harmonics of the order of multiples of three cancel out leading to the elimination of several harmonic components. Thus in the frequency spectrum, no lower order harmonics are present. The lowest order harmonic that appears in the output is of order $m_f - 2$.

The circuit diagram of a three-phase voltage source inverter is shown in Figure 4-6. The operation of the switches M_1 to M_6 is determined by comparing the reference sinusoidal waveform with the carrier triangular wave signal. For the leg *a*, the upper switch M_1 is turned on when $v_{ar} > v_{tr}$ and the lower switch M_4 is switched in a complimentary manner in order to avoid a shoot through. When M_1 is turned on, the output voltage of phase *a* (v_{an}) equals the positive DC link voltage (V_{dc}) and equals the negative DC link voltage (0) when the lower switch is conducting. The phase voltage at the output switches between two levels (V_{dc} and 0) and so the inverter is termed as a two-level inverter.

The duty cycle (Fig. 4.7) generated for the three phases are given by

$$d_a = \frac{v_{an}}{V_{dc}}$$

$$d_b = \frac{v_{bn}}{V_{dc}} \tag{4.8}$$

$$d_c = \frac{v_{cn}}{V_{dc}}\,.$$

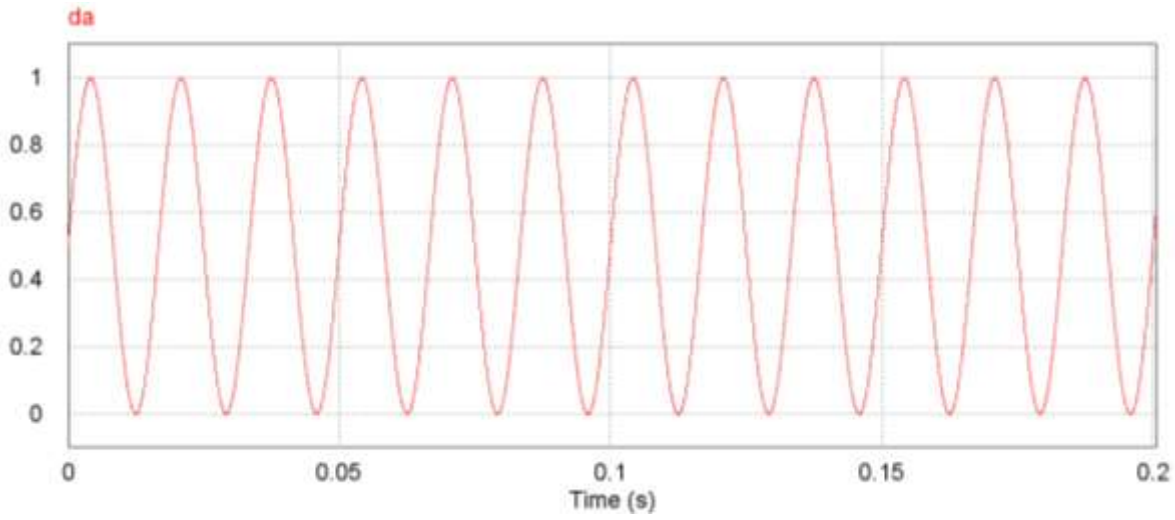

Figure 4-7: Modulating signal for sinusoidal PWM scheme

The maximum amplitude of the fundamental component of the phase voltage in the linear modulation region ($0<m_a\leq1$) is $\frac{V_{dc}}{2}$. Using the relationship for three phase circuits, the maximum amplitude of the line-to-line voltage at the output in the linear modulation region can be calculated as $\sqrt{3}\frac{V_{dc}}{2}$. In general, the peak amplitude of the line-to-line voltage at the output in the linear modulation region is given by equation (4.9):

$$(v_{l-l})_{peak} = m_a\sqrt{3}\frac{V_{dc}}{2} \tag{4.9}$$

where m_a is the amplitude modulation index .

4.4.2 Space vector modulated PWM inverters

In space vector pulse-width modulation (SVPWM) scheme, the utilization of the available DC link input voltage is better. The sine PWM scheme can be thought of as an

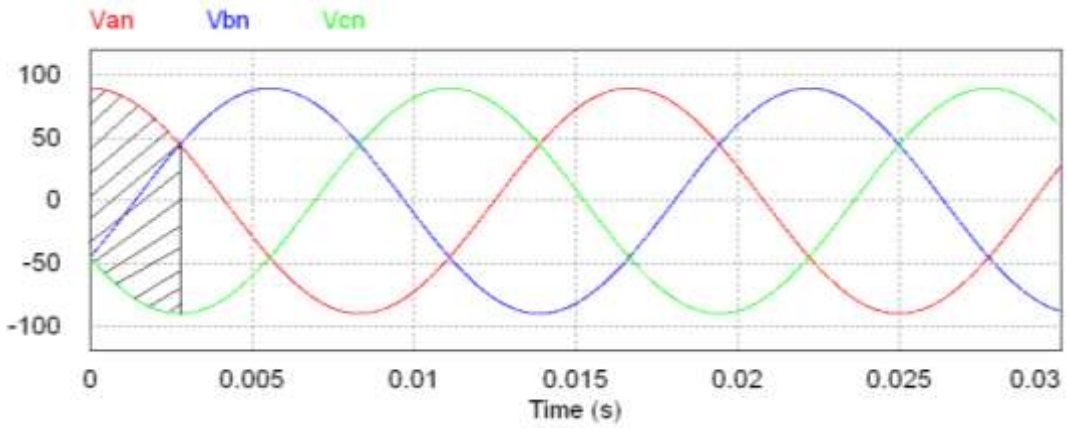

Figure 4-8: Three-phase sinusoidal voltages

operation of three independent phases where the reference signals are generated without consideration of the magnitudes in the other phases. The space vector modulation takes into account the three phase properties of the circuit while generating the reference signal and is more of a real-time modulation technique.

A balanced three-phase sinusoidal voltage is shown in Figure 4-8. A complete cycle of 360° electrical can be subdivided into six equal segments (each having a span of 60° electrical) where one of the three phase voltages has the highest value, one is in the middle, and the third has the lowest value. In the first such 60° span, the voltage of phase *a* (v_{an}) is highest and that of phase *c* (v_{cn}) is lowest. An additional voltage term ($v_k(t)$) consisting of the average of the maximum and minimum of the three phase voltages is injected into the modulating sinusoidal wave used for comparison. For the first 60° span, the term $v_k(t)$ equals the mean of v_{an} and v_{cn}. So, for any instant of time, the additional injected voltage term is given by [25]:

$$v_k(t) = (-\frac{1}{2})[\max(v_{an}, v_{bn}, v_{cn}) + \min(v_{an}, v_{bn}, v_{cn})] \quad (4.10)$$

Hence, the duty cycles (Fig. 4-9) of the switching signals are given by

$$d_a = \frac{v_k(t)}{V_{dc}} + \frac{v_{an}}{V_{dc}}$$

$$d_b = \frac{v_k(t)}{V_{dc}} + \frac{v_{bn}}{V_{dc}} \tag{4.11}$$

$$d_c = \frac{v_k(t)}{V_{dc}} + \frac{v_{cn}}{V_{dc}}\,.$$

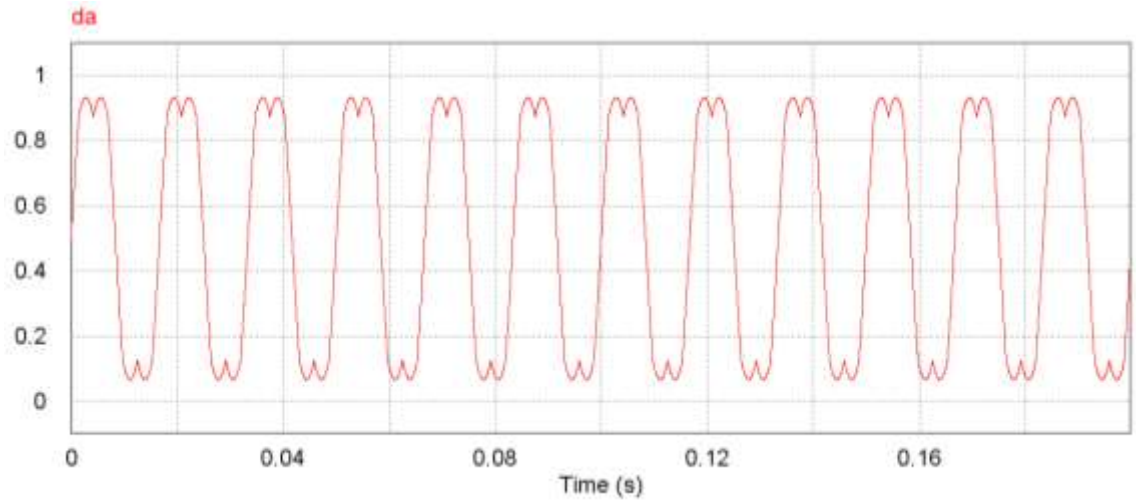

Figure 4-9: Modulating signal for space-vector PWM scheme

The additional term in the duty-cycle equations increases the average area of the modulating waveform and results in an increased output voltage level. The maximum line-to-line output voltage possible using SVPWM scheme is V_{dc} which is greater than the maximum value obtained for sine PWM schemes by a factor $\frac{2}{\sqrt{3}}$. The output voltage of the inverter obtained by using SVPWM scheme is approximately 15% more than that obtained by using sine PWM strategy.

The frequency spectrum of the output voltage is better than that obtained using sinusoidal PWM scheme. The lowest order harmonic obtained in this case is of order $m_f - 4$.

4.4.3 Third-harmonic PWM inverters

The third-harmonic PWM scheme is a selected harmonic injection method. The implementation is similar to both sinusoidal and space-vector PWM techniques. In this case, a third harmonic component is injected into a sinusoidal waveform in order to generate the reference signal (Fig. 4.10). The amplitude of the injected third-harmonic component is

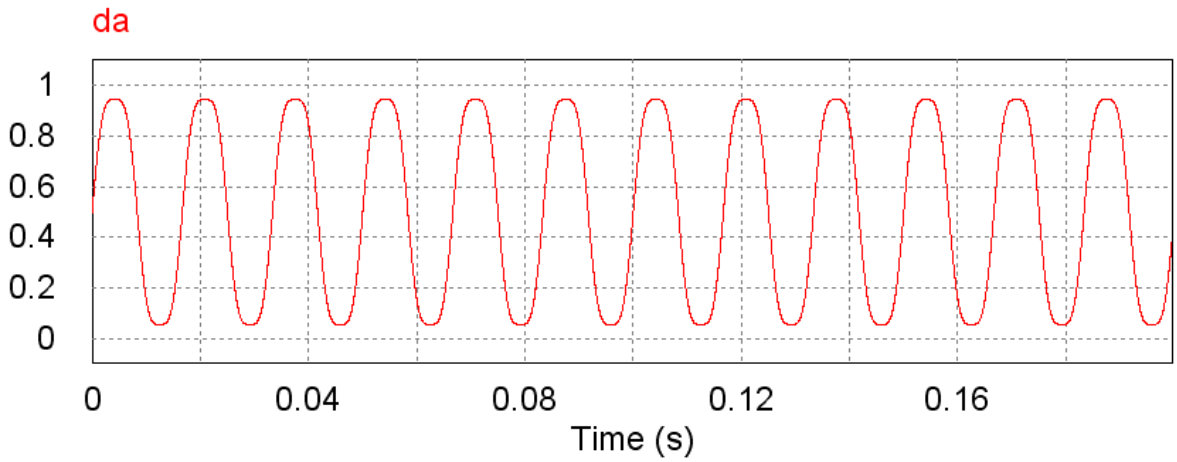

Figure 4-10: Modulating signal for third-harmonic PWM scheme

chosen to be one-ninth of that of the fundamental sinusoidal waveform. The peak value of the reference signal is lower than that for a pure sinusoidal signal, similar to the space-vector PWM scheme. The magnitude of the output voltage is higher than that obtained for sine-PWM scheme but is lower than that obtained for SV-PWM method. The output waveform has the lowest harmonic of the order of $m_f - 4$ and the harmonic profile is better than that obtained for sine-PWM.

A comparison of the results obtained through simulation using PSIM software [30] for the three pulse-width modulation schemes discussed in this section are shown in Table 4-1. The power circuit of inverter shown in Fig. 4.6 was used for the comparison and the input DC link voltage was set at 200V. It can be seen that the peak amplitude obtained for the SV-

PWM method is highest and that for sine-PWM is lowest. Also, the total harmonic distortion (THD) value is lower for the other two schemes compared to sine-PWM method. The implementation of the sine-PWM method is simple but the other two are relatively complex. The third-harmonic PWM method is more complex as an additional third-harmonic component has to be externally generated where as in case of SV-PWM method the additional component ($v_k(t)$) is derived from the reference three-phase sinusoidal waveforms. The amplitude of the carrier triangular wave is chosen to be a little lower than that for sine-PWM method in order to achieve a higher fundamental component for a given DC link voltage.

TABLE 4-1: COMPARISON OF DIFFERENT PWM SCHEMES

Parameter	**Sinusoidal PWM**	**Space Vector PWM**	**Third-Harmonic PWM**
Fundamental peak	172 V	182.4 V	181.6 V
Total harmonic distortion (THD)	68.61%	62.95%	63%
Lowest order harmonic (LOH)	$m_f - 2$	$m_f - 4$	$m_f - 4$

4.5 Conclusions

In this chapter, the various power electronic converters used in renewable energy conversion systems have been discussed. The rectifier used in this work is an uncontrolled diode rectifier. There are two DC-DC converters in the complete hybrid system and each of them has a different topology. They are primarily chosen to provide output voltages from both the wind and photovoltaic systems that match the terminal voltage of the battery which is used as a storage element in this hybrid system. The wind energy system has a low-speed PMSG whose output voltage is lower than that of the battery level. Therefore, a boost topology is used for the DC-DC

converter in the wind system. An MPPT method has been implemented for the PV system whose output voltage widely varies with the level of insolation. Hence, in this case the suitable topology for the DC-DC converter is the buck-boost. A comparison of the three different PWM schemes (Table 4-1) for the three-phase inverter shows that the best possible scheme is the space-vector modulation and this scheme has been implemented in the practical system.

CHAPTER 5. CHARACTERISTICS OF A PMSG-BASED WIND ENERGY SYSTEM

5.1 Introduction

Wind energy conversion systems (WECS) have witnessed a steady growth in power generation over the last two decades. These systems capture the kinetic energy of the wind through the aerodynamically designed blades of a wind turbine and utilize it to rotate a generator which in turn produces electrical power. The wind turbines and the generators used for wind power conversion are discussed in this chapter.

5.2 Wind Turbine Technology

The wind turbine is indispensable for any wind power conversion system. It basically acts as the prime mover for the electrical generator which is coupled to its shaft. The wind turbines are classified as horizontal or vertical axis wind turbines based on their orientation and also as fixed or variable speed wind turbines depending on their mode of operation.

5.2.1 Horizontal and vertical axis wind turbines

The wind turbines are categorized based on the orientation of the spinning axis of their rotor shaft as horizontal axis wind turbines (HAWT) and vertical axis wind turbines (VAWT). Figure 5-1 illustrates the structure of both vertical and horizontal axis turbines.

In horizontal axis wind turbines, the orientation of the spinning axis of the rotor shaft is parallel to the ground. Most of the wind energy systems in the present day use horizontal axis wind turbines. They have a higher energy conversion efficiency compared to their vertical axis counterparts and have features such as blade pitch angle control for power regulation. But the disadvantage is their high installation cost.

The vertical axis wind turbines have the spinning axis of their rotor shaft oriented perpendicular to the ground. They have lower installation and maintenance costs and can be

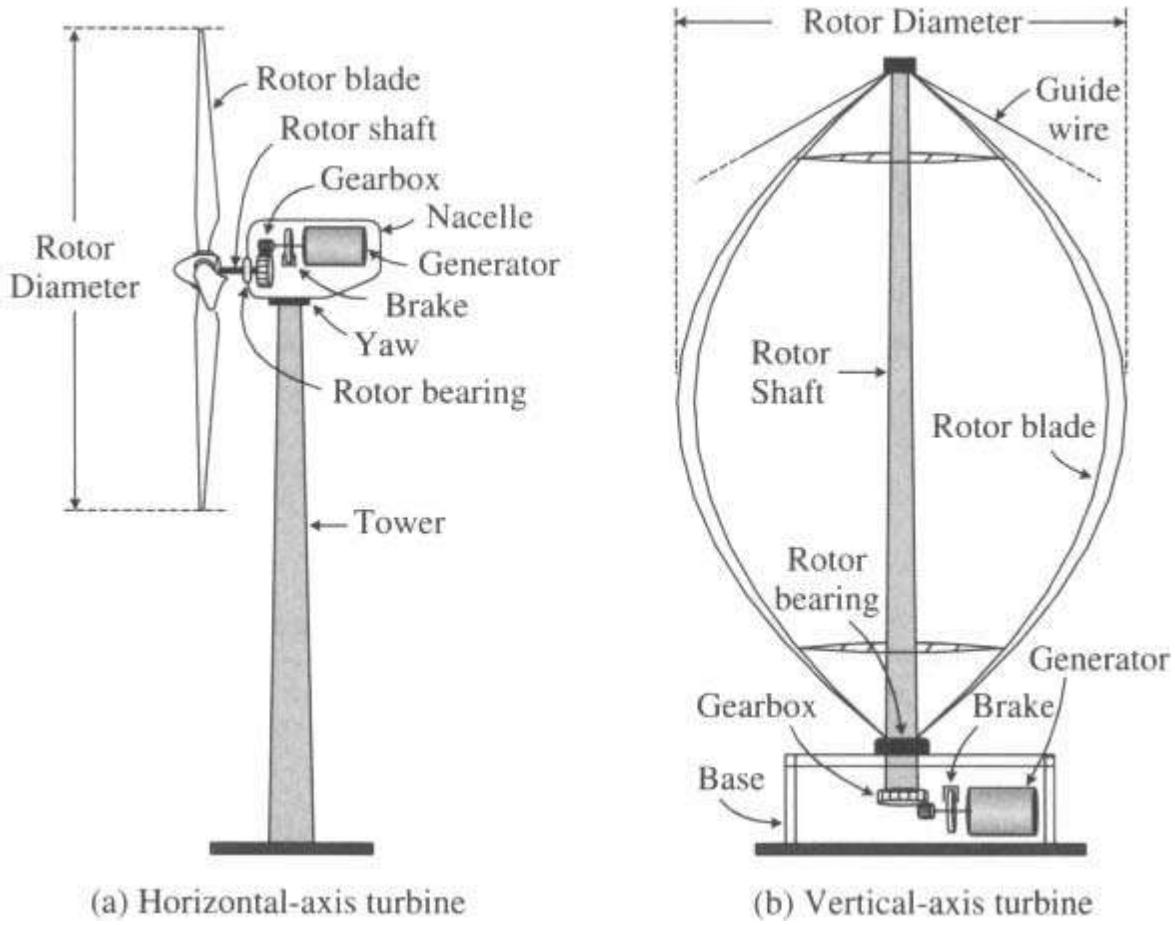

Figure 5-1: Horizontal and vertical axis wind turbines

operated independent of the direction of wind. But on the downside, they have low energy conversion efficiency and are prone to mechanical vibrations leading to higher fluctuations in torque output.

5.2.2 Wind turbine characteristics

The power characteristic of a typical wind turbine is shown in Figure 5-2 [31]. The mechanical power output from a wind turbine is given by [32]:

$$P_m = \frac{1}{2}\rho \Pi R^2 C_p {V_w}^3 \tag{5.1}$$

where P_m is the turbine power, R is the turbine radius, V_w is the wind speed and C_p is the aerodynamic power coefficient which is a function of the pitch angle β and the tip-speed ratio

TSR). In equation 4.1, the terms ρ and R are constant parameters and so the mechanical power output (P_m) from a wind turbine for a particular wind speed (V_w) is maximum only when the

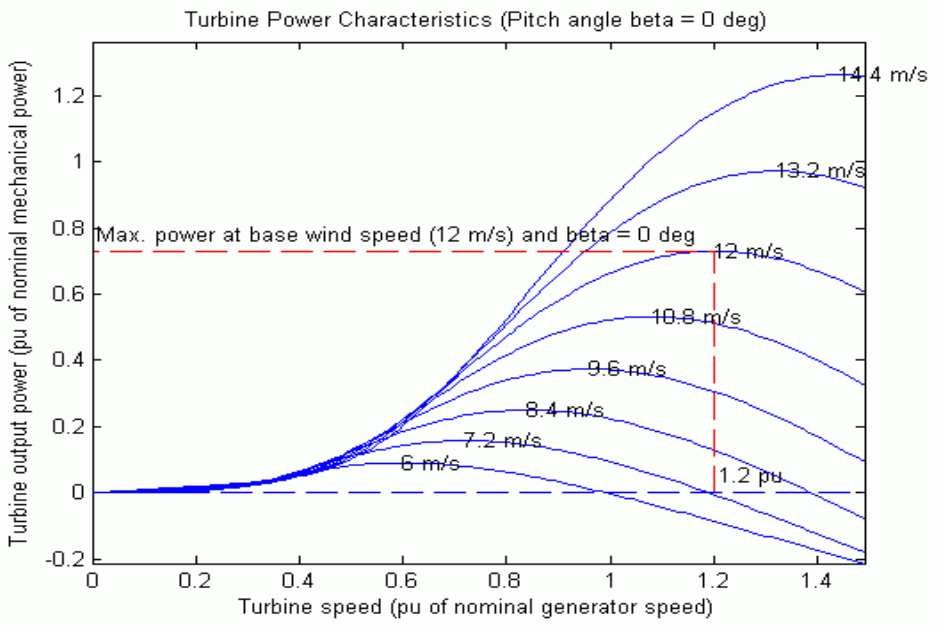

Figure 5-2: Turbine Power Characteristics

aerodynamic power coefficient (C_p) is maximum. Several maximum power point tracking (MPPT) schemes for wind energy systems try to maximize the aerodynamic power coefficient C_p in order to extract the maximum mechanical power from the wind energy for any wind speed. The aerodynamic power coefficient (C_p) is the coefficient of performance of a wind turbine and is influenced by the blade pitch angle and the tip-speed ratio λ which is given by [33]:

$$\lambda = \frac{wR}{V_w} \tag{5.2}$$

where R is the turbine radius and V_w is the wind speed.

A generic equation for C_p based on the turbine characteristics of [32] is given by

$$C_p(\lambda,\beta) = C_1\left(\frac{C_2}{\lambda_i} - C_3\beta - C_4\right)e^{\frac{-C_5}{\lambda_i}} + C_6\lambda \tag{5.3}$$

with $$\frac{1}{\lambda_i} = \frac{1}{\lambda+0.08\beta} - \frac{0.035}{\beta^3+1} \tag{5.4}$$

where β is the blade pitch angle and λ is the TSR.

Figure 5-3 shows the variation of aerodynamic power coefficient (C_p) with tip-speed ratio (λ) as described by equation (5.3). The highest possible value of C_p is referred to as Betz limit. It can be observed from Figure 5-3 that the TSR needs to be maintained at an optimal value for all wind

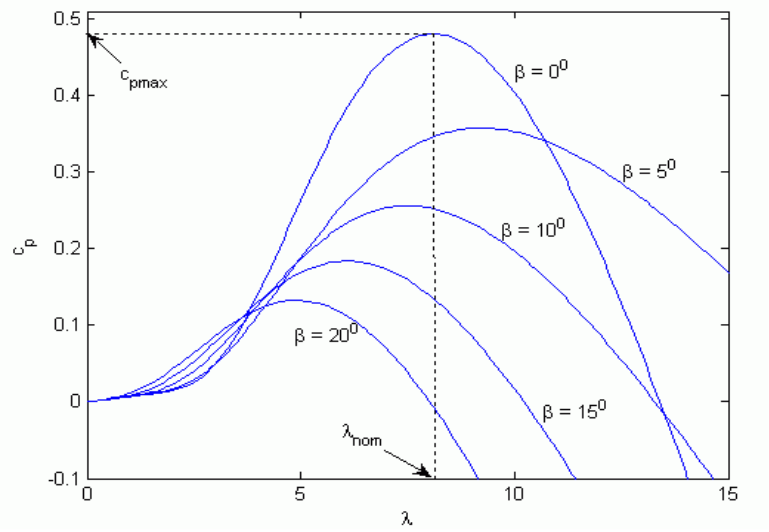

Figure 5-3: C_p versus TSR curve

speeds in order to operate the wind energy conversion system with highest C_p value. This is only possible in variable speed wind energy conversion systems using DFIG or PMSG where the rotor speed of the turbine is adjusted with varying wind speeds in order to maintain the TSR value at the optimal level. Modern wind turbines used for power generation operate at C_p of about 0.4 [16]. In case of small wind turbine generation systems, the blade pitch angle β is rarely changed. However, for large scale wind conversion systems, pitch angle control is used by varying β in order to optimize the power output.

5.3 Doubly-fed Induction Generators

Doubly fed induction generators (DFIGs) are widely used in variable speed wind energy conversion systems (WECSs). DFIG is basically a wound rotor induction generator in which the rotor windings are accessible. The rotor speed can thus be controlled by connecting external components to the rotor terminals in order to achieve variable speed operation. Figure 5-4 illustrates a typical WECS using a DFIG as the generator. The stator is either directly connected to the grid or through a transformer while the rotor is connected to the grid through a transformer. Since the injected rotor power from the grid constitutes about 25% of the output power, a bidirectional back-to-back voltage source converters and a harmonic filter of lower rating are used [15]. The rotor circuit consists of two power converters namely the grid side converter and the rotor side converter and each is controlled separately. The function of the rotor

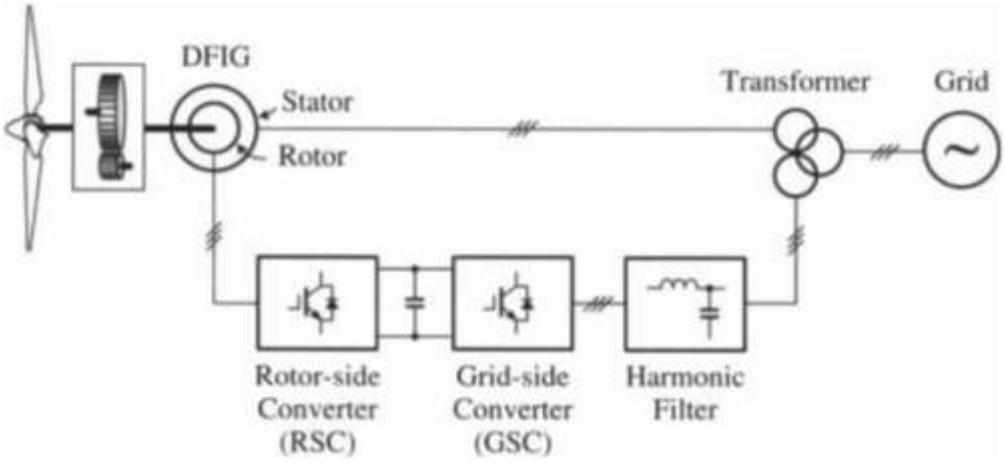

Figure 5-4: DFIG based wind energy system

side converter is to control the active and reactive power of the system by controlling the rotor current components while the main purpose of the grid side converter is to maintain a steady DC link voltage [34]. Since the stator is directly connected to the grid, the stator frequency is

determined by the grid frequency (60Hz). The frequency of the injected rotor current from the grid is controlled in a manner such that the sum of the rotor frequency and the equivalent frequency corresponding to the mechanical rotation equals the stator frequency.

The speed of the DFIG can be varied by about $\pm$33% about the synchronous speed [35]. There are two modes of operation of a DFIG depending on the speed of rotation, namely the sub-synchronous mode and the super-synchronous mode. In the sub-synchronous mode, the generator rotates at a speed below its synchronous speed and the slip for the machine in this case is positive. Under this mode of operation, power is fed into the rotor from the grid. In the super-synchronous mode, the speed of rotation of the generator is above its synchronous value and the slip for this case is negative. The direction of power flow in the rotor circuit is reversed and the grid is fed by the rotor through the power converters. The stator, on the other hand, directly feeds power to the grid under all operating conditions. The relationship between the stator and rotor power is given by

$$P_r = s \times P_s \tag{5.5}$$

where P_r is the rotor power, P_s is the stator power and s is the slip for the induction machine.

DFIG is particularly suitable for variable speed systems as both active and reactive power control can be achieved. But the disadvantage of a DFIG is that it requires a wound rotor with slip rings which results in increased rotor losses.

5.4 Permanent Magnet Synchronous Generators

5.4.1 Overview

Variable-speed wind generation systems are mostly used in the present day in order to extract the maximum energy from the wind at varying wind speeds. Synchronous generators are also used in such systems. These generators can be classified as permanent magnet or wound rotor

generators depending upon the type of excitation systems used. Also, the synchronous generators are classified as salient pole and non-salient pole generators depending on the structure of the poles. The permanent magnet synchronous generators (PMSGs) are particularly suitable for small variable-speed wind turbine generator systems and represent one of the most recent trends in wind power application systems [32]. The PMSGs are designed with large number of poles with smaller pole pitch in order to obtain low operating speeds. The advancements made in the area of magnetic material technology have contributed to the development of permanent magnet machines. The structure of permanent magnet generators is more compact than their wound rotor counterparts as the excitation system constitutes only permanent magnets which require smaller space instead of bulky rotor windings which need to be excited through some external source. The absence of any physical windings in the rotor circuit eliminates any field copper losses thereby making the PMSGs much more efficient than wound rotor generators.

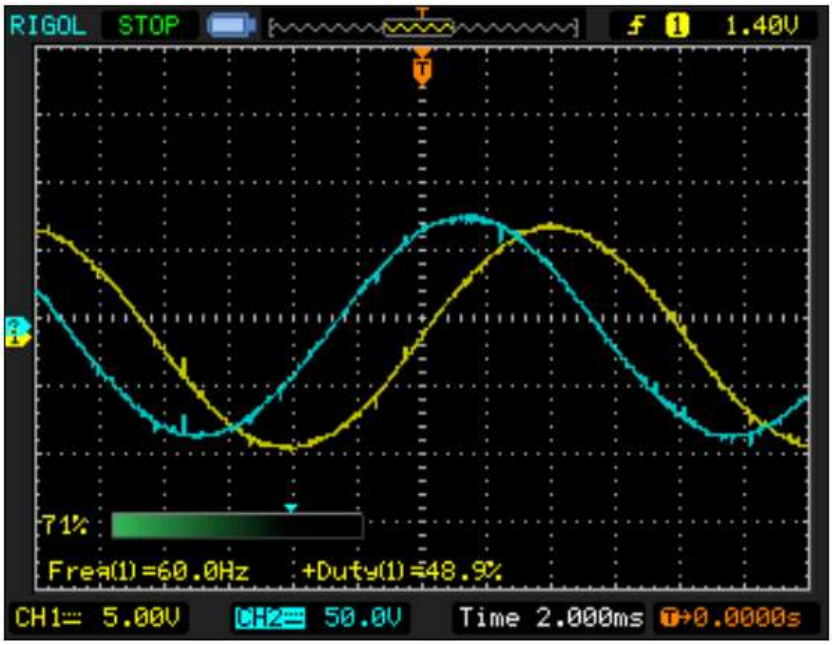

Figure 5-5: Waveforms of $\boldsymbol{V_{ab}}$ and $\boldsymbol{V_{cb}}$ obtained from BLAC

But on the downside, the PMSG cannot be constructed for large ratings because large magnets are not available for constructing machines with high ratings and are thus used for small wind conversion systems only. Smaller wind energy systems generally operate at fixed blade pitch angle of wind turbines and thereby eliminate additional pitch angle controllers.

The PMSGs obtain their field excitation from permanent magnets and are brushless in nature. These machines are operated in the brushless AC (BLAC) mode. The back-emf generated in BLAC machines is essentially sinusoidal in nature (Figure 5-5). However, in some practical machines, the back-emf waveform may depart slightly from sinusoidal nature [36]. The waveform shown in Figure 5-6 shows the output voltage of one phase obtained from another machine. In this case, the waveshape is stepped in nature and is not completely sinusoidal in nature. The brushless machines are radial flux machines and are classified as surface-mounted permanent magnet (SPM) or interior permanent magnet (IPM) machines depending upon the location of the permanent magnets in their rotor [37]. The majority of permanent magnet

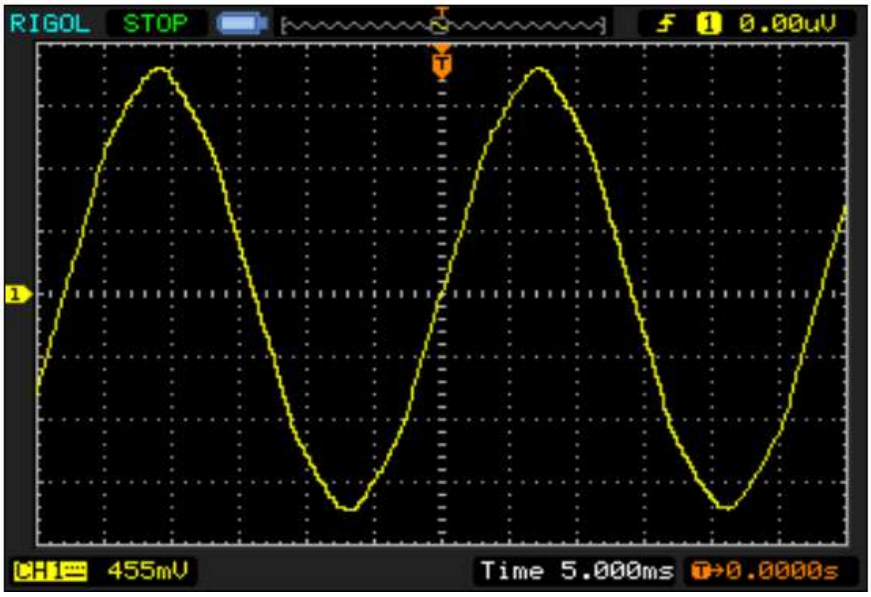

Figure 5-6: Non-sinusoidal back-emf from PMSG

machines are SPM machines. Such machines have equal inductances along both the *d*-axis and *q*-axis. The permanent magnets are mounted on the surface of the rotor and are exposed directly to the demagnetizing effect of armature reaction. The SPM machines have a limited flux-weakening capability and are not suitable for operations above rated speed. The IPM machines have permanent magnets buried inside the rotor iron making them effectively shielded from the demagnetizing effect of armature reaction. The presence of the physical magnet in the rotor makes the value of the *d*-axis inductance smaller than the *q*-axis inductance and results in an additional torque component called the reluctance torque. The machine has a very good performance for constant power operation in the flux-weakening region beyond the rated conditions and is suitable for operation over a wide range of speeds.

The PMSG is normally constructed with a large number of poles so it can operate at a low speed that directly matches the rotational speed of the wind turbine and can thus be connected to the rotor shaft of the wind turbine. Such a directly connected arrangement is referred to as a direct-drive system and does not require additional gearbox arrangements [38]. The elimination of gearbox results in the reduction of installation and maintenance costs and provides an advantage over DFIG based systems where the use of a gearbox is mandatory. The PMSG can cater to a wide range of rotor speeds corresponding to varying wind speeds. The frequency and amplitude of the output voltage obtained at the stator terminals of a PMSG vary with the wind

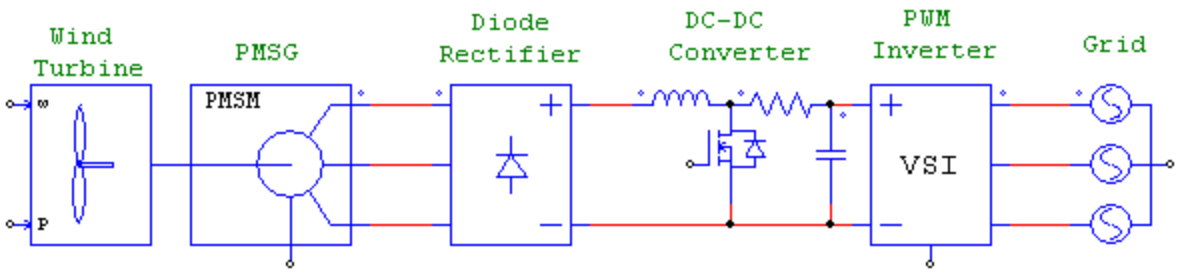

Figure 5-7: PMSG based wind energy system

speed. The stator is connected to the grid using power electronic converters. Figure 5-7 illustrates a typical PMSG based wind energy conversion system. Since there is no additional rotor control involved, the power converters used are rated at full-capacity ensuring maximum wind energy conversion efficiency for wide range of wind speeds. Also, the full-capacity ratings of power converters help to meet various grid codes and do not need additional equipment for fault ride-through condition [15].

5.4.2 PMSG characteristics

The generator used in this thesis work is a PMSG and the details of the machine used and its characteristics for different conditions have been discussed in this section. The machine used is a permanent magnet brushless machine. The waveform of the back-emf is sinusoidal in nature and it is operated in a brushless AC (BLAC) mode. The ratings for the generator under test are presented in Table 5-1.

TABLE 5-1: MACHINE RATINGS

Parameter	**Value**
Rated Power	250 W
Rated Volts	42 Vdc
Max. Speed	4000 RPM
Rated Current	5.7 A
Resistance (line-to-line)	0.19Ω
Inductance (line-to-line)	0.49mH
No. of Poles	10

The steady-state induced voltage for a PMSG is given by [39]

$$E = K_e \omega \tag{5.6}$$

where E is the induced back-emf, ω is the angular speed of rotation and K_e is the back emf constant for the PMSG.

The variation of the line-to-line voltage at the output with speed of rotation of the generator is illustrated in Figure 5-8. The back-emf generated from the machine is sinusoidal in nature. The line-to-line voltages obtained from the generator at a rotational speed of 720 rpm are shown in Figure 5-5. The number of poles of the machine is 10 and hence a speed of 720 rpm corresponds to an operating frequency of 60 Hz.

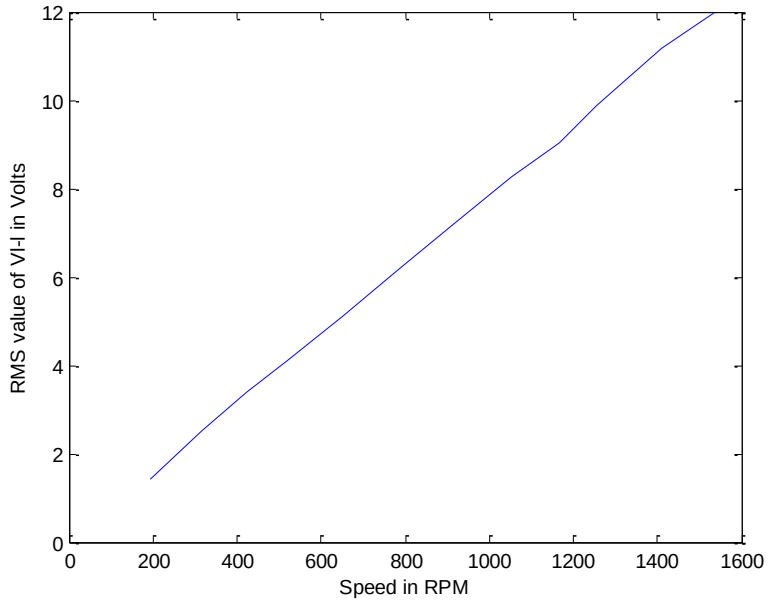

Figure 5-8: Variation of line-to-line voltage with rotational speed

The rms value of the line-to-line voltage at the PMSG output terminals is given by

$$V_{l-l_{rms}} = \frac{\sqrt{3}}{\sqrt{2}} V_m \, . \tag{5.7}$$

The load characteristics of the PMSG illustrating the variation of line-to-line voltage with line current for three different speeds are shown in Figure 5-9. The drop in voltage with increasing load current is due to the increasing internal drop due to stator winding impedances.

The output voltage obtained at the PMSG terminals is fed to a three-phase diode rectifier to obtain a DC voltage. The rectified output voltage (V_{rec}) from the rectifier is given by equation 4.1. The variation of the rectified output voltage with changes in the DC link current is shown in Figure 5-10.

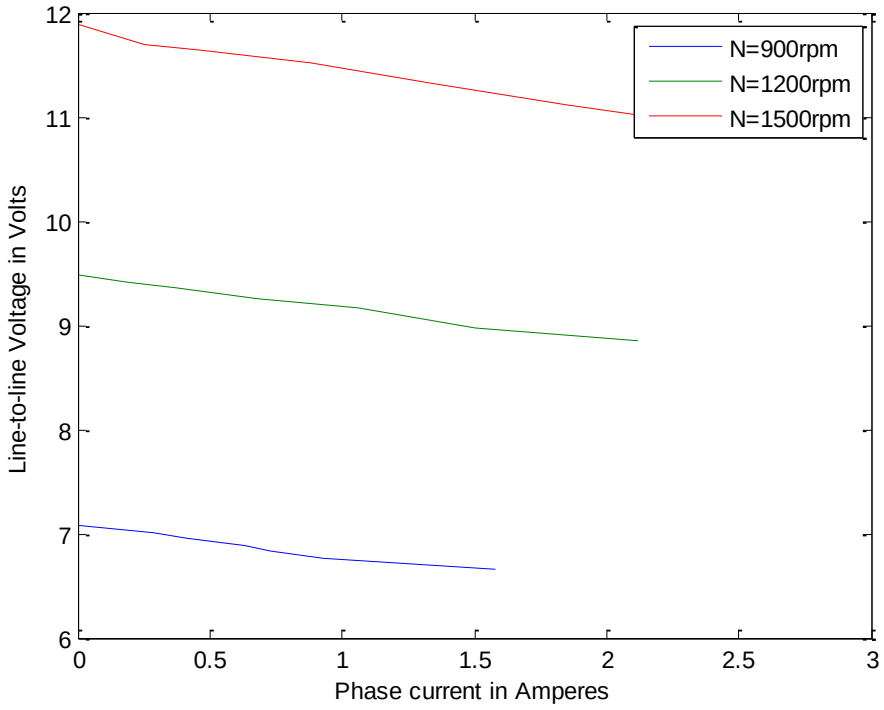

Figure 5-9: Load Characteristics

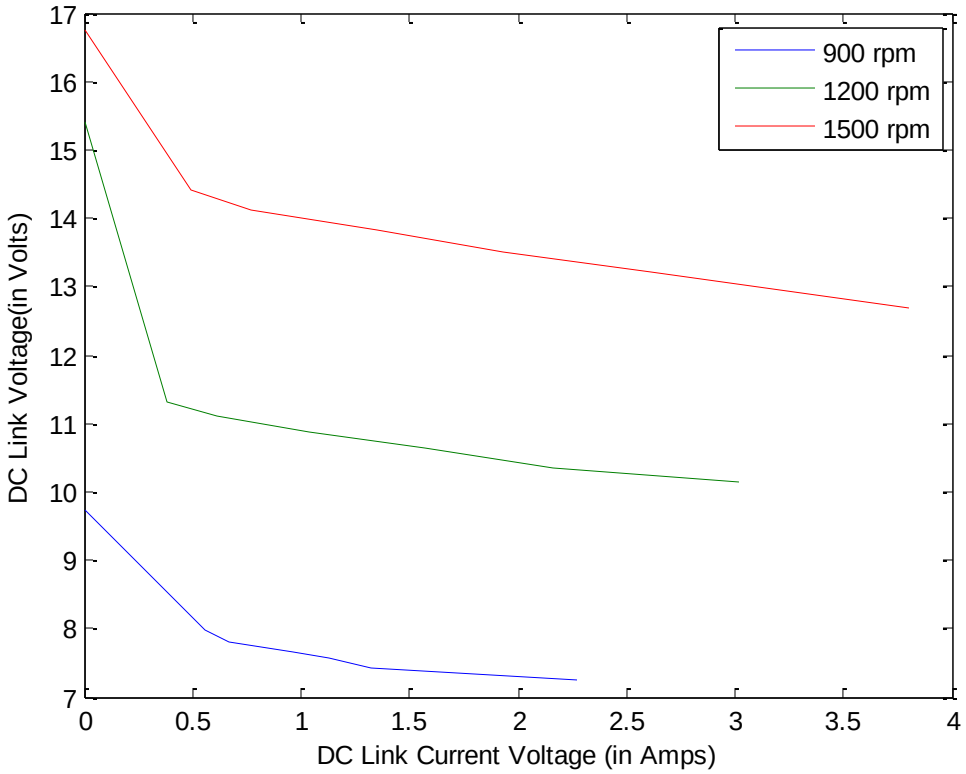

Figure 5-10: V_{rec} versus I_{dc} curve

5.5 Conclusions

In this chapter, the major components used in wind conversion systems such as the wind turbines and the generators were discussed. A comparison between the two most widely used generators in variable-speed wind generation systems, namely a DFIG and a PMSG was made. The system developed in this work uses a PMSG which has been discussed in details. The different types of rotor construction and the output characteristics have also been included in this chapter.

CHAPTER 6. MPPT SCHEME FOR PHOTOVOLTAIC SYSTEMS

6.1 Introduction

In this chapter, a control algorithm for implementing an MPPT scheme for a PV panel has been developed using Simulink. The MPPT equation is derived based on the open-circuit voltage and the short-circuit current of a PV panel [40]. The power circuit for the photovoltaic panel uses a pulse width modulated (PWM) DC/DC buck-boost converter between the solar panel and the load. The MPPT is realized by sensing the short-circuit current and the open-circuit voltage and adjusting the duty-cycle of the buck-boost converter and hence the converter output current such that the MPPT equation holds. The proposed scheme ensures the delivery of maximum power under all environmental conditions. It uses a simple control circuitry for the MPP tracker resulting in an efficient and PV system. The PWM pulses for the DC/DC converter are generated using dSPACE [13].

6.2 Mathematical Analysis

The approximate expression for the output current I_{PV} of a PV panel is given by

$$I_{PV} = I_{SC} - I_S \exp(\mathrm{K}V_{PV}) \tag{6.1}$$

where V_{PV} is the voltage across the PV panel, I_{PV} is the output current, I_{SC} is the short-circuit current, I_S is the dark saturation current, and K is a constant that depends on the temperature and arrangement of cells in the panel.

Rewriting equation (6.1),

$$\mathrm{K}V_{PV} = \ln\left(\frac{I_{SC}-I_{PV}}{I_S}\right). \tag{6.2}$$

The power output of the PV panel is given by:

$$P_{PV} = V_{PV}\, I_{PV}. \tag{6.3}$$

Combining (6.2) and (6.3) we obtain

$$KV_{PV} = I_{PV} \ln(\frac{I_{SC}-I_{PV}}{I_s}). \quad (6.4)$$

For obtaining the maximum power point, (6.4) is differentiated with respect to I_{PV} and equated to zero as

$$\frac{d(KP_{PV})}{dI_{PV}} = \ln(\frac{I_{SC}-I_{PV}}{I_s}) - (\frac{I_{PV}}{I_{SC}-I_{PV}}) = 0. \quad (6.5)$$

Substituting (6.2) into (6.5) and solving

$$I_{SC} = (\frac{1}{KV_{MP}} + 1)\, I_{MP} \quad (6.6)$$

where V_{MP} and I_{MP} are the voltage and current at the maximum power point.

At the maximum power point, the following result is obtained from (6.1):

$$I_{MP} = I_{SC} - I_S \exp(KV_{MP}). \quad (6.7)$$

The substitution of (6.6) into (6.7) yields

$$I_{MP} = I_{SC} - I_S \exp(\frac{I_{MP}}{I_{SC}-I_{MP}}) \text{ or}$$

$$I_{MP} = (I_{SC} - I_{MP}) \ln(\frac{I_{SC}-I_{MP}}{I_S}). \quad (6.8)$$

6.2.1 Exact approach

The dark saturation current of the PV panel in (6.1) can be expressed as [3]:

$$I_S = I_{or}(\frac{T}{T_r})^3 exp[\frac{qE_{go}}{Bk}(\frac{1}{T_r} - \frac{1}{T})] \quad (6.9)$$

where I_{or} is the cell's reverse saturation current at a reference temperature T_r=298K, T is the temperature of panel in Kelvin, E_{go} is the band gap for Silicon in eV, q is the charge of an electron, B is ideality factor and k is Boltzmann's constant.

Equation (6.9) can be rewritten as

$$I_s = I_{or}(\frac{T}{T_r})^3 \exp[K_1 - K_1 \frac{T}{T_r}] \quad (6.10)$$

where $K_1 = \frac{qE_{go}}{BkT_r}$.

Equation (6.10) can be expressed as

$$\frac{1}{I_s} = A\frac{\exp(K_1\frac{T}{T_r})}{T^3} \quad (6.11)$$

where $A = \frac{{T_r}^3}{I_{or}\exp(K_1)}$.

Equation (6.11) can be rewritten as

$\ln(\frac{1}{I_s}) = \ln A - 3\ln T + K_1\frac{T_r}{T}$ or

$$\ln(\frac{1}{I_s}) = \ln A - 3\ln T + \frac{C}{T} \quad (6.12)$$

where C is a constant equal to K_1T_r.

Substituting (6.12) into (6.8)

$$I_{MP} = (I_{SC} - I_{MP})\left[\ln(I_{SC} - I_{MP}) + \ln A - 3\ln T + \frac{C}{T}\right] \quad (6.13)$$

Equation (6.13) gives an implicit relationship between I_{MP} and I_{SC} (at maximum power point). Sensing I_{SC} and adjusting I_{MP} such that equation (6.13) holds is an accurate way of tracking the MPP of the solar panel.

The open-circuit voltage at temperature T can be expressed as

$$V_{OC}(T) = V_{OC}(T_r) + \alpha(T - T_r) \quad (6.14)$$

where $V_{OC}(T)$ is the open-circuit voltage at temperature T, $V_{OC}(T_r)$ is the open-circuit voltage at a reference temperature T_r, and α is the temperature coefficient of V_{OC}.

Substituting for T from (6.14) into (6.13),

$$I_{MP} = (I_{SC} - I_{MP})\left[\ln(I_{SC} - I_{MP}) + \ln A - 3\ln\left(\frac{V_{OC}(T) - V_{OC}(T_r)}{\alpha} + T_r\right) + C\left(\frac{\alpha}{V_{OC}(T) - V_{OC}(T_r) + \alpha T_r}\right)\right] . \quad (6.15)$$

This is the exact equation that can be used to track the maximum power point of a PV panel.

6.2.2 Approximate approach

To simplify the implementation of (6.15), certain approximations have been made. The term $[\frac{T}{T_r}]^3$ in (6.9) can be approximated to 1 in the practical temperature range of the PV panel and thus the term I_{or} exp $[\frac{qE_{go}}{Bk}(\frac{1}{T_r}-\frac{1}{T})]$ describes the approximate variation of I_s with temperature. With the above approximation, the accuracy of tracking the maximum power point will be quite acceptable. Equating $[\frac{T}{T_r}]^3$ in (6.9) to 1 and then substituting into (6.7) yields

$$I_{MP} = (I_{SC} - I_{MP})\left[ln(I_{SC} - I_{MP}) + ln\, B + \frac{C}{T}\right] \tag{6.16}$$

where B is a constant and equal to $\frac{1}{I_{or}exp(K_1)}$.

Substituting (6.14) into (6.16)

$$I_{MP} = (I_{SC} - I_{MP})\left[ln(I_{SC} - I_{MP}) + ln\, B + C\left(\frac{\alpha}{V_{OC}(T)-V_{OC}(T_r)+\alpha T_r}\right)\right]. \tag{6.17}$$

Equation (6.17) can be rewritten as:

$$I_{MP} = (I_{SC} - I_{MP})\left[\ln(I_{SC} - I_{MP}) + B_1 + (\frac{C_1}{V_{OC}(T)-A_1})\right] \tag{6.18}$$

where $A_1 = V_{OC}(T_r) - \alpha T_r$, $\quad B_1 = \ln B \quad$ and $\; C_1 = \alpha C$.

Hereafter equation (6.18) will be called "MPPT-Equation". The performance of the MPPT system implementing (6.18) should be quite satisfactory. Figure 6-1 illustrates the design of the power circuit and the necessary control algorithm.

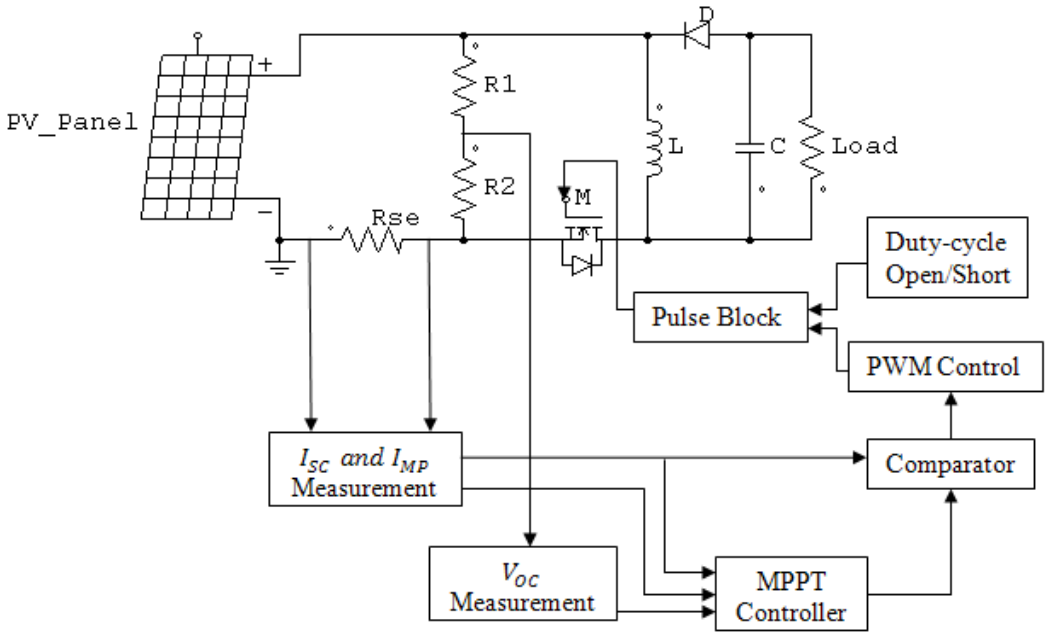

Figure 6-1: Power Circuit with Control Scheme

6.3 Control Scheme using dSPACE

The Simulink model of the control scheme implementing equation (6.18) is shown in Fig. 6-2. Equation (6.18) suggests that in order to implement the MPPT equation, the short-circuit current and the open-circuit voltage of the panel need to be sensed at regular intervals of time [41]. The current and voltage are sensed through the blocks DS1104ADC_C5 and DS1104ADC_C6 respectively. Both the blocks are connected to the output ports of the dSPACE controller board CP1104. The same block DS1104ADC_C5 is used for sensing both the instantaneous current values and the short-circuit current. The blocks "V_{oc} Measurement" and "I_{sc} Measurement" (Fig. 6-2) measure the values of V_{oc} and I_{sc} once in an interval of 800ms and hold the values until the next measurement takes place. The normal PWM pulses to the MOSFET M generated by the control scheme is interrupted for a period of 2300μs in an

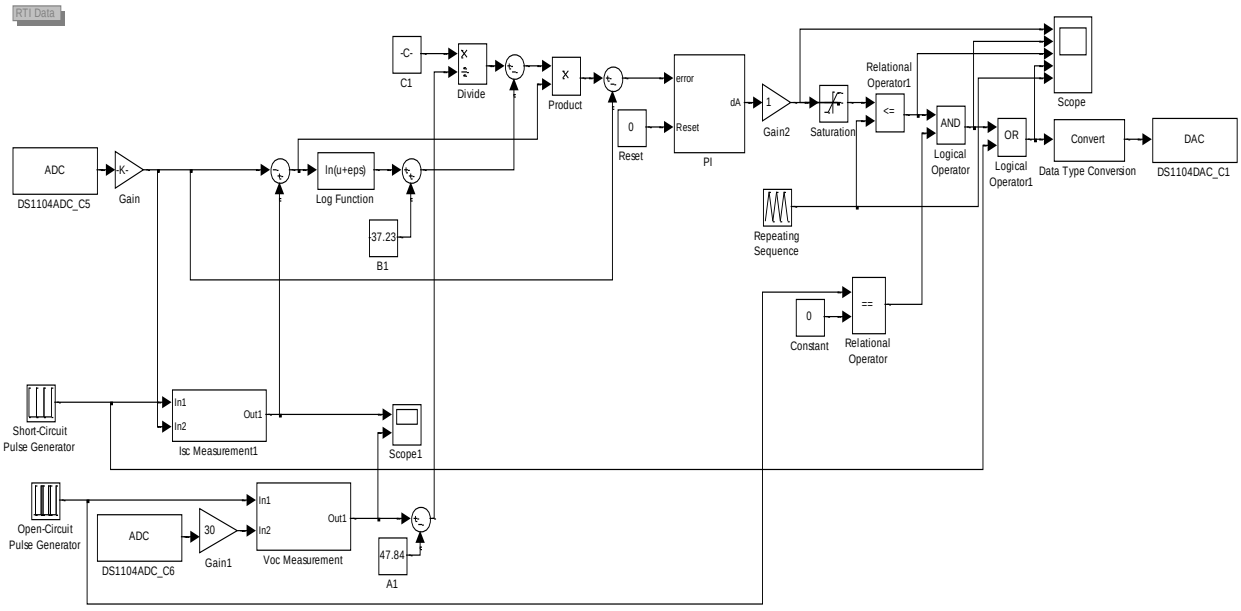

Figure 6-2: Simulink Model for Control Scheme

interval of 800ms for measuring the values of V_{oc} and I_{sc}. The measuring period is divided into two separate durations within each 800ms block. The first duration of 800µs is used for I_{sc}Measurement. A long pulse is applied to the MOSFET during this time so that the inductor current reaches its steady-state value and this current represents the short-circuit current. During the second duration of 1500µs of the measuring period, the pulses to the MOSFET are blocked and this condition represents the open-circuit state. The open-circuit voltage V_{oc}(T) is measured across R_2 using the potential divider arrangement. The intervals of 800us and 1500us are sufficient time to allow the circuit to reach steady-state condition so that both V_{oc} and I_{sc} measurements are done correctly. In our case the measuring period is only 2300µs in an interval of 800ms such that the PV power is unavailable for a negligible 0.29% time.

In the Simulink model, the two blocks "Short-circuit Pulse Generator" and "Open-circuit Pulse Generator" generate pulses of durations 800µs and 1500µs respectively once in every 800ms. The pulses of "Short-circuit Pulse Generator" are fed as the on-time pulse for "I_{sc} Measurement" block for recording the short-circuit current (Fig. 6-2). The "I_{sc} Measurement" subsystem of Simulink model is shown in Fig. 6-3. There are two inputs to the subsystem. The first input (In 1) is the output of "Short-circuit Pulse Generator" and the second input (In 2) is the value of current measured as a voltage across the resistance R_{se}. The block "Switch Case Action Subsystem I" collects the value of In 2 until the pulse (In 1) is high and gives the last stored value of In 2 as the output of "I_{sc} Measurement" subsystem once the pulse (In 1) goes low. The "V_{oc} Measurement" subsystem is exactly the same as the "I_{sc} Measurement" subsystem. The on-time pulse for "V_{oc} Measurement" block generated by the "Open-circuit Pulse Generator" serves as In 1, and In 2 is the voltage measured across R_2.

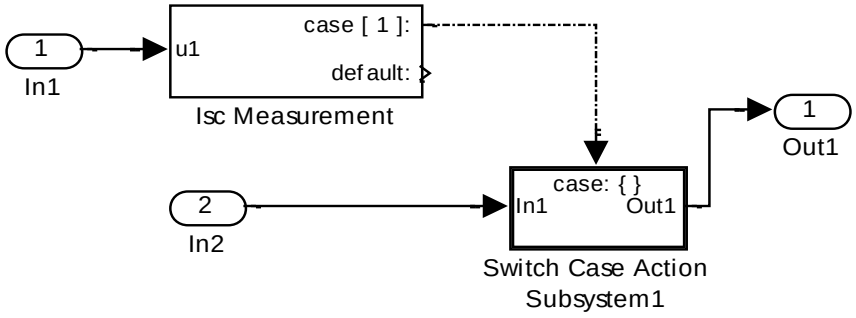

Figure 6-3: "I_{sc} Measurement" block in Simulink

The inverse (complement) of the output of "Open-circuit Pulse Generator" block and the PWM pulses are first passed through logic AND operation to ensure that no pulses are fed to MOSFET M during open-circuit voltage measurement. The resulting signal is added (through logic OR operation) with the output of "Short-circuit Pulse Generator" to generate the long

pulse needed to measure the short-circuit current. The resulting signal is the final gate signal to the MOSFET M which is sent out through the block DS1104DAC_C1.

6.4 Panel Calculations

The proposed MPPT algorithm is implemented on a 15W PV panel. The maximum short-circuit current value of the panel is 1A. The panel is made of polycrystalline silicon for which the E_{go}value is 1.21eV. The reverse saturation current value for the panel at a reference temperature of 298K is given as 50μA. The temperature coefficient of V_{oc} for the panel is -80mV/K and the $V_{oc}(T_r)$ value at T_r= 298K is 24V for the panel. The constants for the panel A_1, $B_1$and C_1 are calculated using the panel parameters as

A_1= 47.84; B_1= -37.23 and C_1= -1123.72.

The power versus voltage characteristics of the solar panel under test are plotted for five different values of insolation using MATLAB. The different insolation levels were obtained by varying the distance of the panel from the sun-simulator lamps (two 1kW lamps serving as the source of light). The level of insolation decreases with increasing distance of the panel from the light source while all other ambient conditions remain the same.

The characteristics for the panel are shown in Fig. 6-4 in which the insolation level 1 is highest and 5 is the lowest. The corresponding values of open-circuit voltage and short-circuit current for the five levels are:

V_{oc1}= 24.13V and I_{sc1}= 1.061A;

V_{oc2}= 23.03V and I_{sc2}= 0.86A;

V_{oc3}= 21.84V and I_{sc3}= 0.579A;

V_{oc4}= 21.85V and I_{sc4}= 0.405A;

V_{oc5}= 21.66V and I_{sc5}= 0.308A

where suffices 1,2,3,4 and 5 correspond to the five insolation levels.

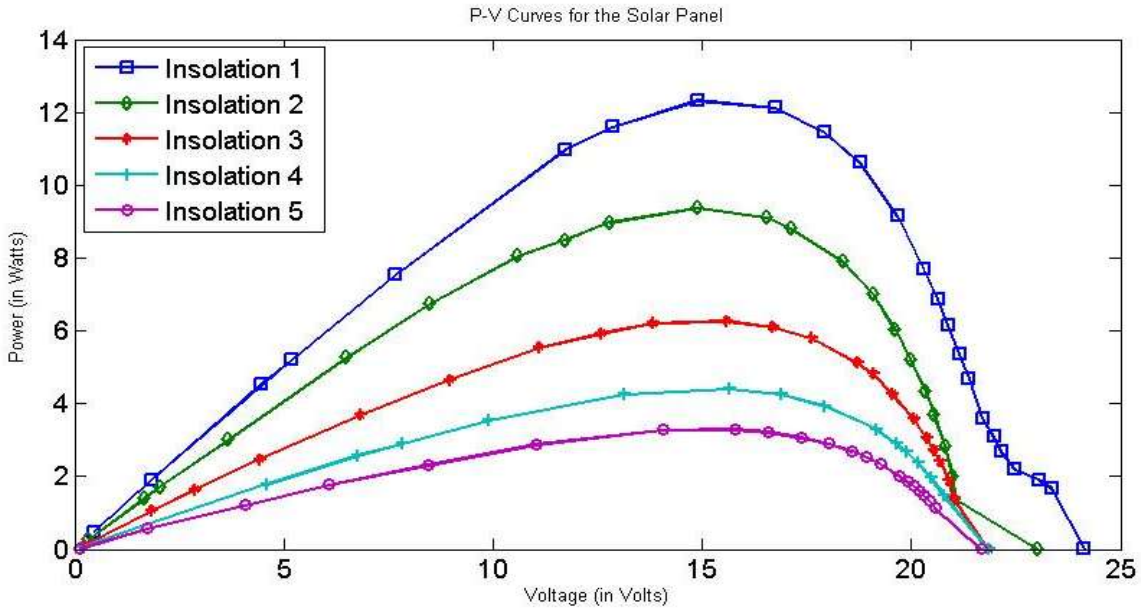

Figure 6-4: Power-versus-voltage curves for the PV panel

6.5 Experimental Set-up and Results

The power circuit of the proposed scheme is shown in Fig.6-5. The output voltage of the panel is applied to the buck-boost converter made up of the MOSFET M, inductor L, capacitor L and diode D as shown in Fig.6-5. Between the panel and the DC/DC converter, a small resistance $R_{se}$is inserted for current measurement. Also, the potential divider assembly consisting of R_1 and R_2 is used for measuring the open-circuit voltage $V_{oc}(T)$. The buck-boost topology has been chosen to supply a certain output voltage from input voltages higher or lower than the output voltage. In Fig.6-5, the load shown is a resistor and the power converter

operates in the buck mode. For applications such as charging batteries at higher voltage levels, boost action is required.

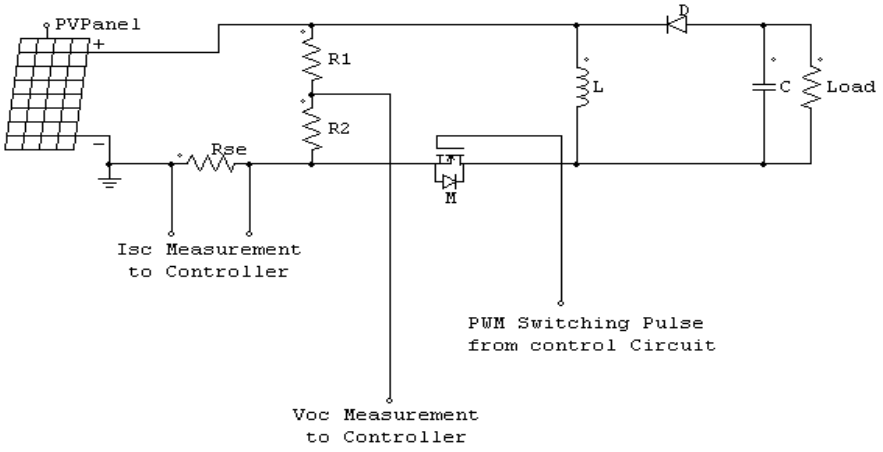

Figure 6-5: Power Circuit Diagram for the Scheme

The proposed control scheme was implemented using dSPACE. The same five insolation levels used for plotting the panel characteristics were maintained for testing the MPPT scheme. The values of the maximum power obtained from the panel at the above insolation levels during testing have been tabulated (Table 6-1) and compared with the values of maximum power point (MPP) at the corresponding levels of insolation during tracking.

TABLE 6-1: MAXIMUM POWER POINT VALUES

Insolation Level	**Maximum Power from Characteristics (in Watts)**	**Maximum Power tracked by the Scheme (in Watts)**
1	12.33	11.28
2	9.38	8.43
3	6.27	5.11
4	4.42	4.2
5	3.3	3.3

The gate pulses generated for triggering the MOSFET are shown in Fig. 6-6. Also, a snapshot of the dSPACE Control Desk layout depicting the gate signals for MOSFET and the values for the short-circuit current and open-circuit voltage are presented in Fig. 6-7.

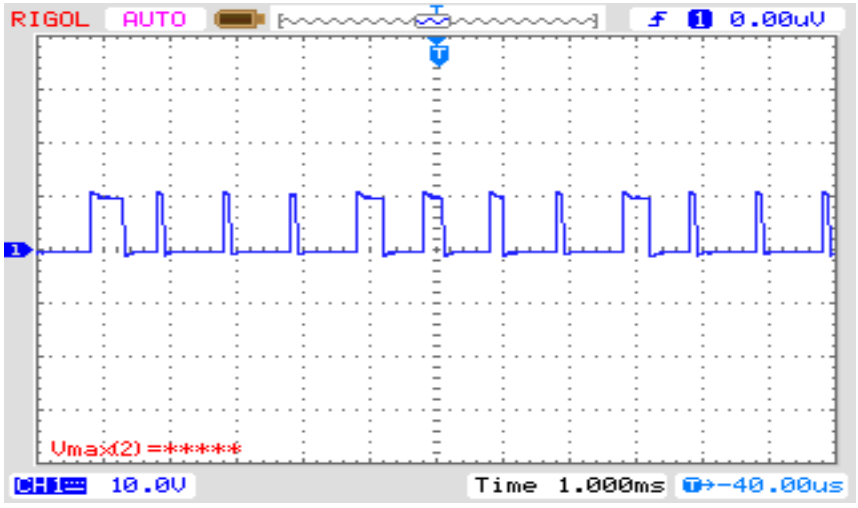

Figure 6-6: Gate Signals for MOSFET

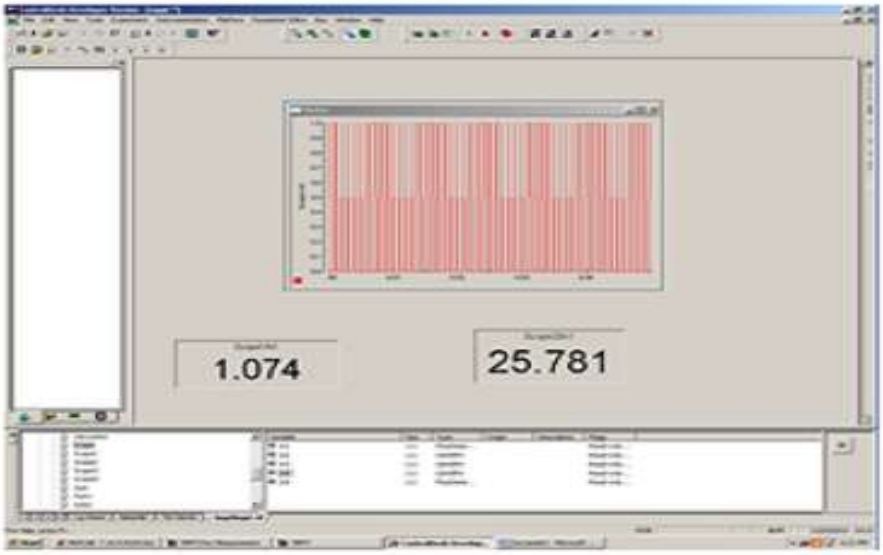

Figure 6-7: Gate pulses and V_{oc} and I_{sc} values from dSPACE Control Desk

6.6 Conclusions

An accurate MPPT method using the open-circuit voltage and short-circuit current has been implemented using dSPACE. The ‘MPPT equation’ used also includes the effect of temperature. The small discrepancies in the maximum power values can be attributed to the use of approximate MPPT equation instead of the actual one. This scheme is particularly suitable for small PV systems since the implementation is simple.

CHAPTER 7. HYBRID RENEWABLE ENERGY SYSTEM WITH WIND TURBINE AND PV PANELS

7.1 Introduction

The photovoltaic system discussed in Chapter 6 was integrated with a wind energy conversion system. However, a SEPIC converter is used in the PV system instead of a buck-boost converter for DC-DC conversion in order to address the polarity issues for the hybrid scheme. Section 7.2 elaborates the wind energy conversion system which forms part of the hybrid scheme. Figure 7.1 shows the schematic diagram for the complete hybrid system. Both

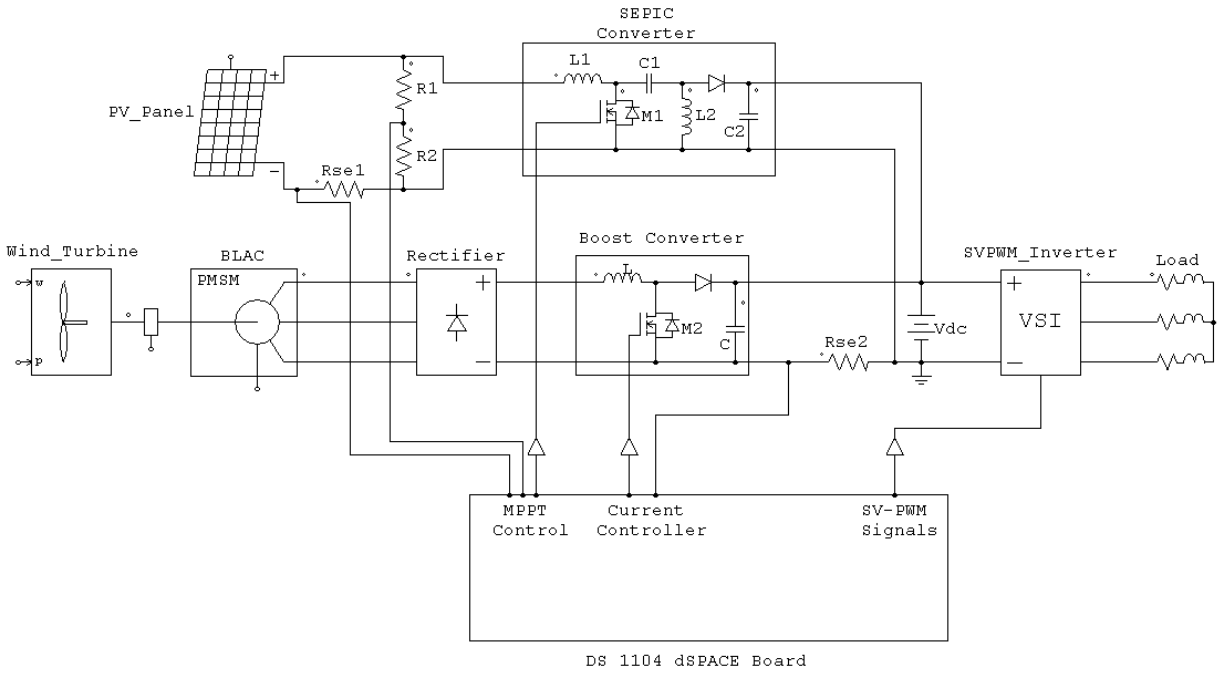

Figure 7-1: Schematic Diagram for the complete Hybrid System

the wind generator and the PV panel share a single DC link and this configuration eliminates an additional inverter for AC conversion. A 12 V battery is connected to the DC link in order

to store the excess energy and also to provide additional energy in absence of sunlight. The details of the hardware circuit and the results obtained are presented in this chapter.

7.2 Controller for Wind System

The wind energy subsystem uses a PMSG as the electric generator. The machine is essentially a brushless AC (BLAC) machine used in the generator mode of operation. The specifications for the machine have been provided earlier in Chapter 5. The wind turbine is replaced with a DC motor in the actual experimental set-up. The DC motor is directly coupled to the shaft of the BLAC and it acts as the prime mover for the electric generator in the experimental hardware set-up. The wind energy subsystem is integrated with the photovoltaic set-up at the DC link. A battery is connected across the DC link. Now, in order to connect the wind subsystem to the battery link, the output voltage of the subsystem is to be matched to the battery voltage. This is obtained using a controller for the DC-DC converter in the wind

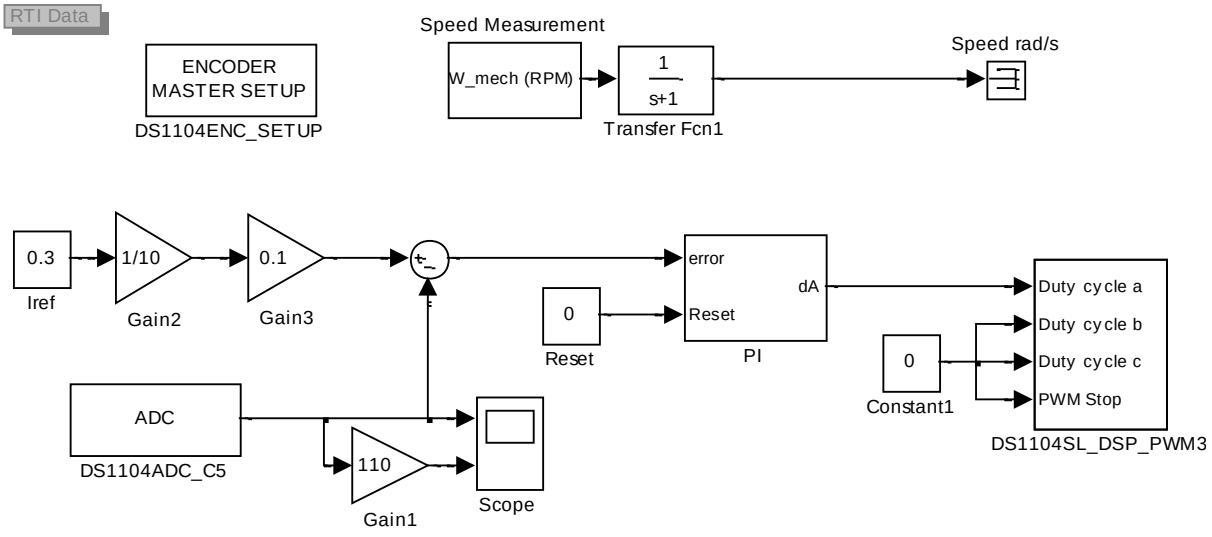

Figure 7-2: Simulink Model for DC Link Current Controller of Wind Energy System

energy conversion system. The DC-DC converter has a boost topology since the PMSG operates at low speeds and the output voltage needs to be stepped up. The DC link voltage level is determined by the battery voltage and a current controlling scheme is used to select the DC current supplied by the wind energy subsystem. The controller is implemented using Simulink and dSPACE. The Simulink model for the controller is shown in Fig. 7.2. The current is sensed as a voltage across a sensing resistance (R_{se_2}) of value 0.02Ω and is fed to the DS 1104 board using port ADCH 7. The signal is multiplied with proper gains in order to get the value of current. The signal is multiplied by a factor of 500 to take into account the value of resistance (0.02Ω) and also an inherent gain of 10 for DS1104 board. The value of the sensed current is compared with a reference value (0.3A) and the error is passed through a PI controller. The PI controller is implemented in Simulink and its output is used to generate the duty cycle for the MOSFET (M_2). The duty cycle value is fed to PWM 3 block which compares the duty cycle with an internal carrier triangular wave signal inside the slave DSP of DS 1104. The carrier frequency is specified as 10 kHz. The generated pulses from the slave DSP has a peak level of 5 V only and is insufficient for triggering the MOSFET which needs a 10 V pulse for turning on. Also, the source of the MOSFET M_2 is not directly connected to the ground of the hardware circuit. The current sensing resistance (R_{se_2}) is connected in between the source of M_2 and the ground. Thus it becomes necessary to isolate the switching signals for the MOSFET M_2 in order to avoid any ground loop currents. To overcome the problem, an additional driver circuit arrangement shown in Figure 7-3 is used. The generated pulses from the slave DSP are passed through a hex-buffer IC (SN7407N) and the output is pulled up to the 10 V level using a pull-up resistor. The output of the buffer at pin 2 is connected to an opto-coupler IC (H11AA1) through a small resistance (30Ω) in order to

isolate the signals. The output transistor of the opto-coupler has an open-collector arrangement and is powered from a separate 10V source. The gate signals for the MOSFET (Figure 7-4) are obtained at the emitter at pin 6. The reference current is matched in the actual hardware and the voltage level of the DC link is already determined by the battery voltage of 12.5 V.

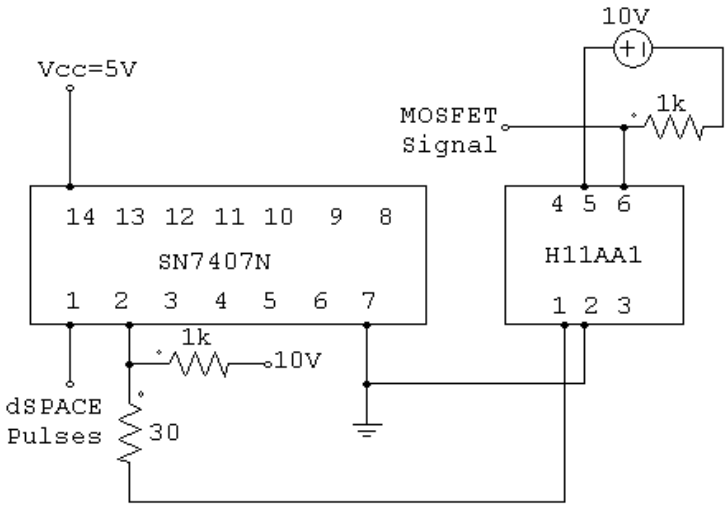

Figure 7-3: Driver Circuit for MOSFET M_2

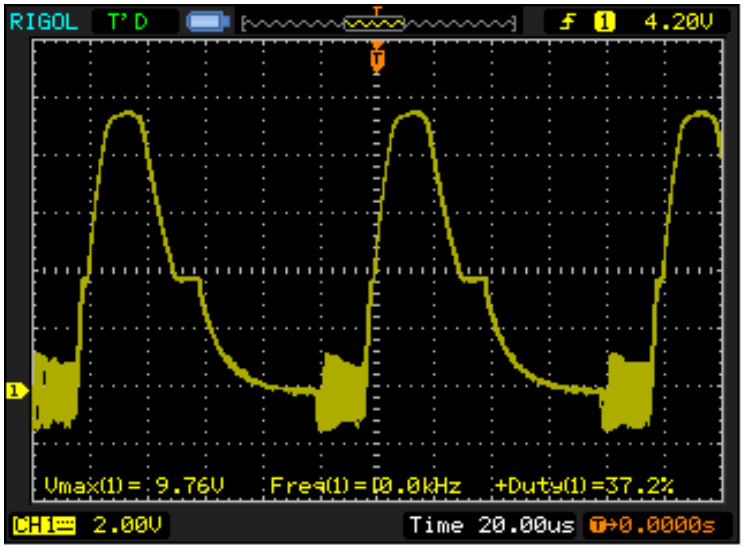

Figure 7-4: Switching signals for MOSFET M_2

7.3 Operation of Hybrid System using MPPT Technique for PV Subsystem

The photovoltaic subsystem following a MPPT algorithm (as discussed in Chapter 6) is implemented in the hybrid system. In order to integrate the PV subsystem with the wind conversion subsystem, a few changes to the hardware set-up of the PV subsystem were made. The negative bus of the DC link serves as the ground for the entire system. In order to keep the output polarity of the PV subsystem same as the wind subsystem, a SEPIC is used as the DC-DC converter instead of a buck-boost converter. The SEPIC converter provides an output voltage with the same polarity as its input unlike a buck-boost converter. This also helps to eliminate any ground loop current for the different sensing elements used as the entire control for the hybrid system was generated in Simulink (Figure 6-2) and implemented using a single DS 1104 dSPACE hardware board. The ground for the dSPACE board is the same as the hardware circuit ground. The open-circuit voltage and the short-circuit current measurements are carried out as discussed in Chapter 6 using the single switch (M_1). V_{oc} measurement is

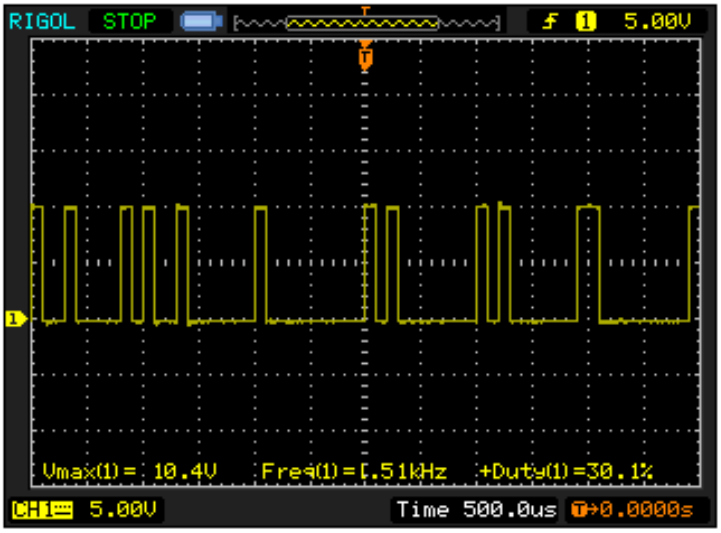

Figure 7-5: Switching signals for MOSFET M_1

done using a potential divider arrangements using resistances R_1 and R_2, each of which has a value of 1 MΩ while I_{sc} measurement is carried out using the sensing resistance (R_{se_1}). The voltage and current signals that are sensed are multiplied by appropriate gains in order to account for the gains of the sensors and the dSPACE board. The gains obtained for V_{oc} and I_{sc} measurements are 20 and -200 respectively. The gate pulses generated for MOSFET M_1 of the SEPIC converter for MPPT operation are shown in Figure 7-5.

7.4 Experimental Results

The complete hybrid system was implemented in hardware. Figure 7-6 shows the experimental set-up. The system was tested for two different light levels. The PV panel was

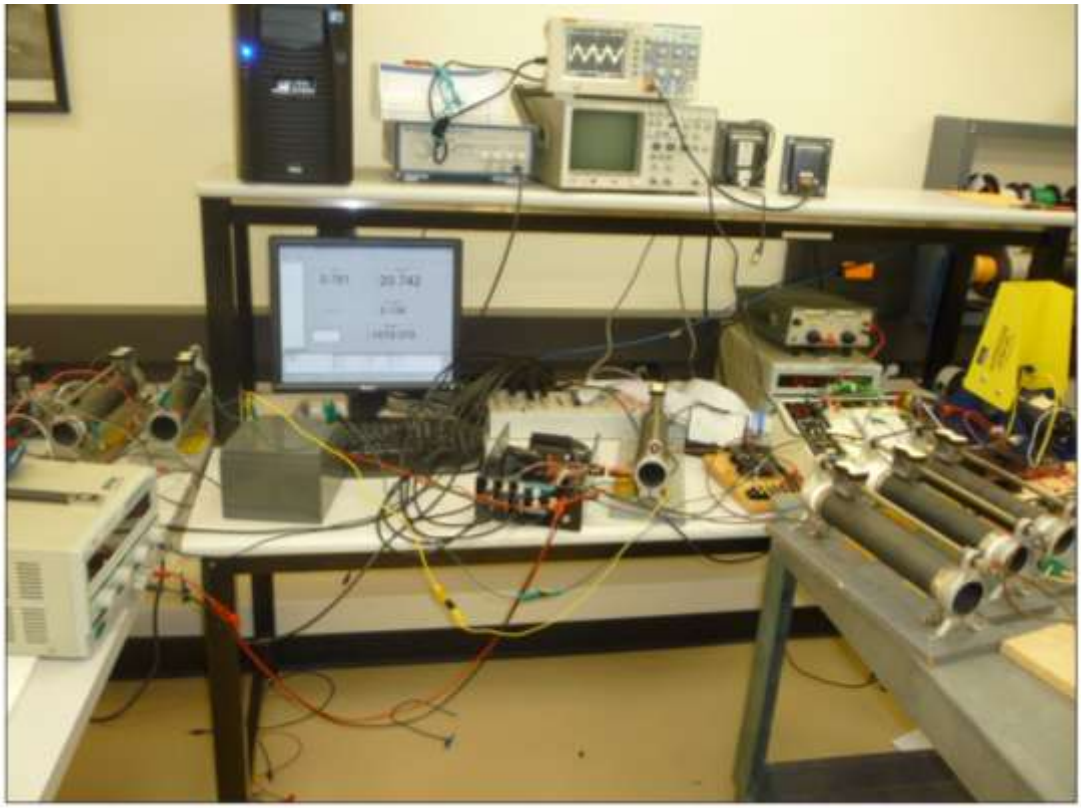

Figure 7-6: Experimental Set-up for the Hybrid Power Conversion Scheme

subjected to two insolation levels 1 and 2 (corresponding to the same light intensity level as

TABLE 7-1: EXPERIMENTAL RESULTS

CASE I	Insolation Level	1
	PV Panel Current	1.12A
	PV Panel Voltage	10.92V
	PV output power	12.23W
	I_{PV} supplied by PV subsystem	0.31A
	PMSG Speed	965 rpm
	V_{l-l} output from PMSG	7.52 V
	V_{rec} output	8.59 V
	I_W supplied by wind energy subsystem	0.3 A
	Battery voltage	13.8 V
	V_{l-l} output from inverter	6.2 V
CASE II	Insolation Level	2
	PV Panel Current	0.785A
	PV Panel Voltage	9.85V
	PV output power	7.73W
	I_{PV} supplied by PV subsystem	0.12A
	PMSG Speed	953 rpm
	V_{l-l} output from PMSG	7.32 V
	V_{rec} output	8.27V
	I_W supplied by wind energy subsystem	0.3A
	Battery voltage	13.2V
	V_{l-l} output from inverter	5.81V

discussed in Chapter 6). The PMSG speed was kept constant and the reference current for the wind controller was set at 0.3A. The results obtained for the above two cases are shown in Table 7-1.

SV-PWM Inverter

The three-phase inverter used in this work is implemented using space-vector pulse-width modulation technique. A separate module using the IC IRAM136-3063B with 6 IGBTs and a driver is used. The driver IC needs a separate 15V power supply. The DC input terminals of

the inverter are connected to the battery terminals. The switching signals for the inverter are generated using Simulink and dSPACE. The pulses for the six switches are generated in

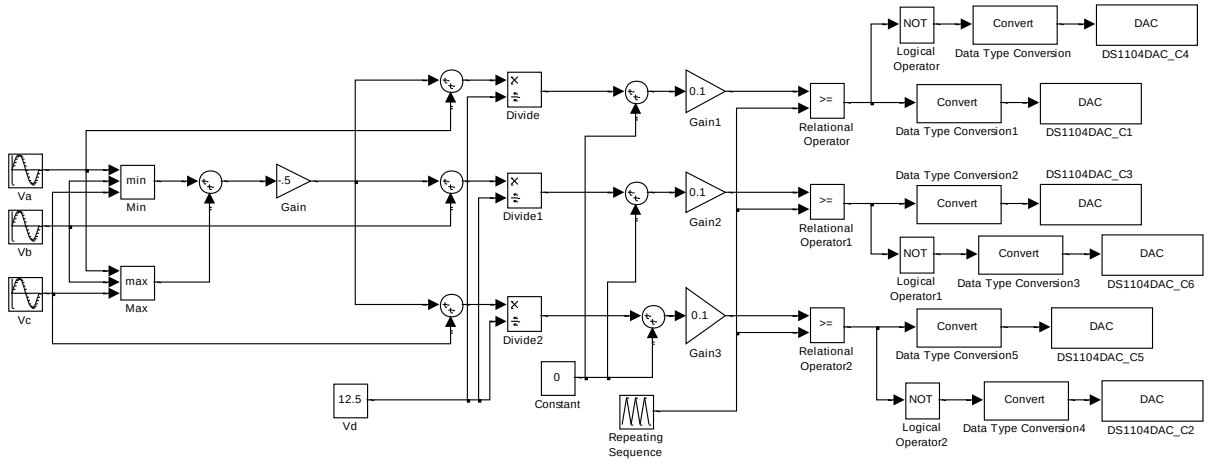

Figure 7-7: Simulink Model for SV-PWM Pulse generation

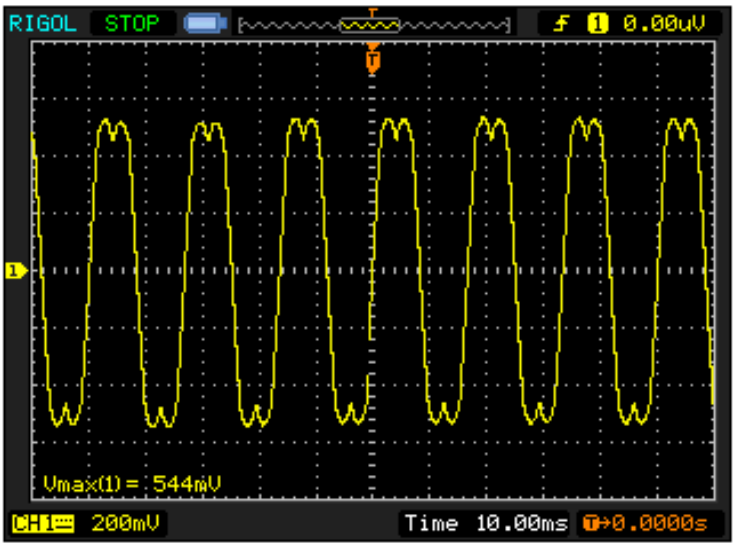

Figure 7-8: Modulating signal for SV-PWM operation

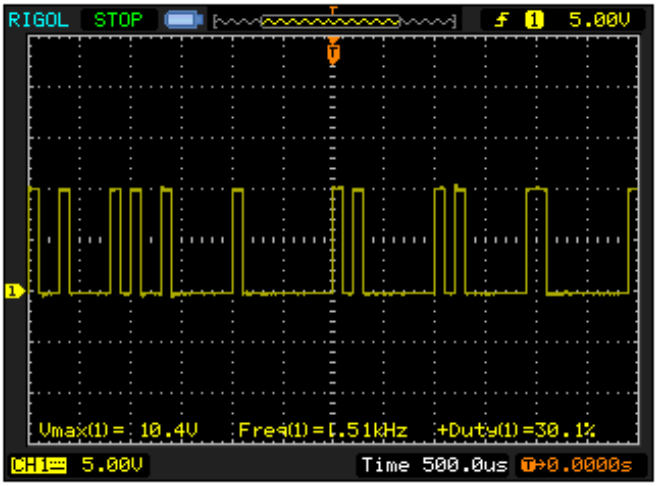

Figure 7-9: Generated pulses for Inverter switches

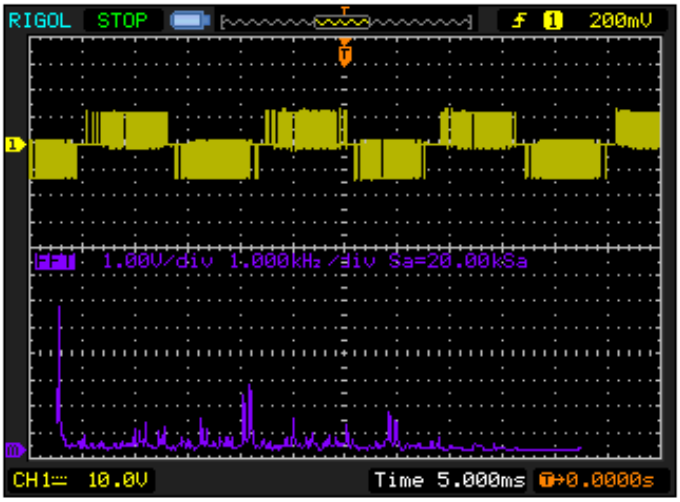

Figure 7-10: Line-to-line output voltage of inverter and its FFT

Simulink following equation (4.11) (Figure 7-7) and implemented using dSPACE hardware (DACH1 through DACH6). The frequency of the carrier triangular wave is kept at 1800Hz. The modulating signal generated for SV-PWM switching is shown in Figure 7-8 and the gate pulses generated for one of the MOSFET switches is shown in Figure 7-9. The waveforms of the AC output voltage and its frequency spectrum obtained for case I are shown in Figure 7-10. The line-to-line output voltage is measured to be 6.2V rms and THD value obtained from

the FFT of the waveform is calculated to be 84.2%. The lowest order harmonic is 26 (i.e. of the order of $m_f - 4$) and occurs at a frequency of 1560 Hz. A three-phase balanced R-L load is connected to the output of the inverter. Three rheostats connected in series with 680µH inductances serve as the three-phase load. The current waveform has considerable amount of high frequency distortion which can be reduced by increasing the inductance values. The THD

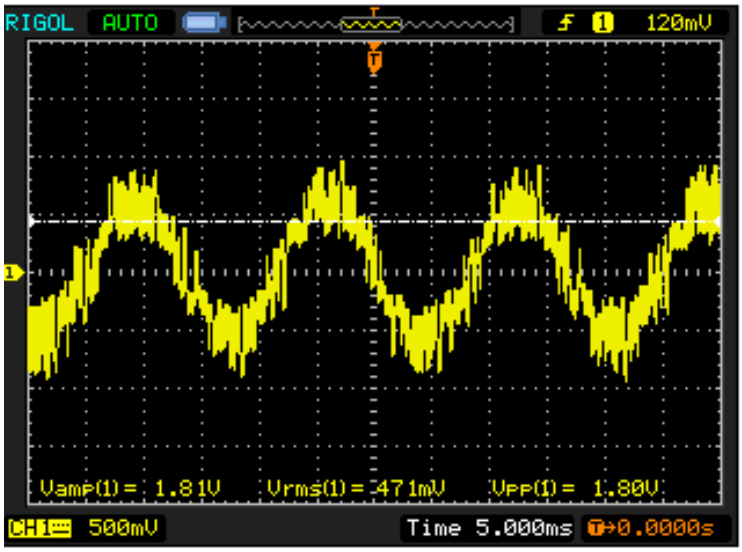

Figure 7-11: Line Current Waveform for R-L Load

for the current waveform is 24.9%. The resistances are set at lower values to increase the current amplitude to 1A and the waveform obtained is shown in Figure 7-11. A Control Desk layout showing the different readings for the hybrid energy conversion system is shown in Figure 7-12.

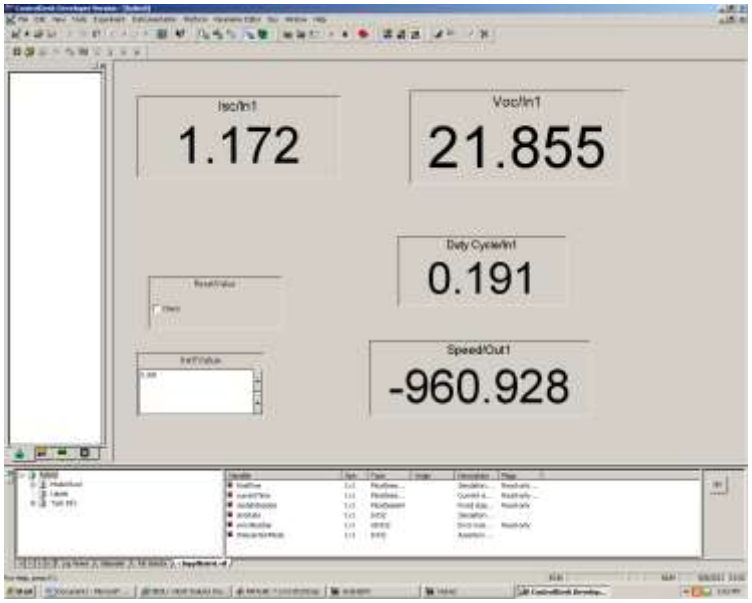

Figure 7-12: Control Desk Layout for Case I

7.5 Conclusions

The complete hybrid power conversion scheme was implemented in hardware and it was found that the power obtained using MPPT is close to that obtained from the actual panel characteristics in Chapter 6 (Figure 6-4). Also, in Figure 7-12, it is seen that the reference value of current set for wind energy subsystem is 0.3 A and the current obtained under actual experimental conditions is also of the same value. Even though the output voltage obtained from SV-PWM inverter has a large harmonic content, a sinusoidal current can be obtained using a suitable filter inductance.

CHAPTER 8. CONCLUSIONS

8.1 Review of the Work Done

The thesis work presents a hybrid power conversion scheme which combines both wind and photovoltaic energy sources. The photovoltaic system is provided with maximum power point tracking feature. The MPPT equation is derived from the PV panel characteristic equation and it includes the effect of temperature variation. The MPPT scheme is more accurate compared to fractional short-circuit current and fractional open-circuit voltage methods and thus makes the system more efficient. The wind energy system is controlled to achieve voltage and power matching conditions at its output. A 12 V battery is used to store the excess energy from the photovoltaic system during daytime and also to supply any additional energy to the load in absence of sunlight. The wind and PV systems have DC-DC converters in order to regulate the output voltage. Each of the two systems has a separate topology for the DC-DC converter depending on the operation and also the switching signals for the converters are generated accordingly. The wind system uses a boost converter while the photovoltaic system uses a SEPIC converter for DC-DC conversion. The topology selection has been carried out carefully in order to have the wind and photovoltaic units share a common DC link. The diodes present in the two DC-DC converters prevent any circulating current at the DC link. This configuration does not require two separate inverters for AC conversion which is normally used in hybrid systems having wind and PV sources. The single three-phase inverter used in this hybrid system for converting the DC output into an AC output is implemented using space-vector pulse-width modulation technique which results in a higher output voltage amplitude for a given DC input voltage and a lower THD value than a conventional sinusoidal PWM inverter. The salient feature of this work lies in the fact that the

entire system is implemented in hardware with a single DSP-based control unit. The control system is modeled in MATLAB-Simulink environment, thereby making the system more flexible and is interfaced with the actual hardware system using DSP-based DS 1104 dSPACE hardware board.

8.2 Scope for Future Work

The hybrid system designed in this work is a stand-alone one feeding an isolated R-L load. Additional control for regulating the output voltage may be incorporated. This system can also be modified for grid integration in which case it is possible to control the active and reactive powers fed to the grid. Such integration needs the use of harmonic line filters in order to achieve better output waveform quality. Furthermore, multi-level inverters can be used to provide higher efficiency and lower THD values.

The wind energy conversion system does not have any maximum power point tracking features like its photovoltaic counterpart and so an MPPT control may be incorporated for the wind energy system in order to make the overall power system more efficient.

REFERENCES

[1] E. Spooner and A. C. Williamson, "Direct coupled, permanent magnet generators for wind turbine applications," *Proc. Inst. Elect. Eng.-Elect. Power Appl.,*vol. 143, no. 1, pp. 1-8, 1996.

[2] K. Tan and S. Islam, "Optimal Control Strategies in Energy conversion of PMSG Wind Turbine System without Mechanical Sensors," *IEEE Transactions on Energy Conversion,* vol.19, no. 2, pp. 392-399, June 2004.

[3] C. Hua, J. Lin and C. Shen, "Implementation of a DSP-controlled photovoltaic system with peak power tracking," *IEEE Transactions on Industrial Electronics,* vol.45, pp. 99-107, Feb. 1998.

[4] Y. Kuo, T. Liang and J. Chen, "Novel maximum-power-point-tracking controller for photovoltaic energy conversion system," *IEEE Transactions on Industrial Electronics,* vol.48, pp. 594-601, June 2001.

[5] M.A.S. Masoum, H. Dehbonei and E.F. Fuchs, "Theoritical and experimental analysis of photovoltaic system with voltage and current based maximum power point tracking," *IEEE Transactions on Energy Conversion,* vol.17, pp. 514-522, Dec. 2002.

[6] T. Noguchi, S. Togashi and R. Nakamoto, "Short-current pulse-based maximum power point tracking method for multiple photovoltaic and converter module system," *IEEE Transactions on Industrial Electronics,* vol.49, pp. 217-223, Feb. 2002.

[7] Y. Chen and K.M. Smedley, "A cost-effective single-stage inverter with maximum power point tracking," *IEEE Transactions on Power Electronics,* vol.19, no. 5, pp. 1289-1294, Sept. 2005.

[8] E. Koutroulis, K. Kalaitzaki and N.C. Voulgaris, "Development of a microcontroller-based, photovoltaic maximum power point tracking control system," *IEEE Transactions on Power Electronics,* vol.16, pp.46-54, Jan. 2001.

[9] K.K. Tse, B.M.T. Ho, H.S. Chung and S.Y.R. Hui, "A comparative study of maximum-power-point trackers for photovoltaic panels using switching-frequency modulation scheme," *IEEE Transactions on Industrial Electronics,* vol.51, pp. 410-418, April 2004.

[10] dSPACE *DS 1104 R&D Controller Board: Hardware Installation and Configuration,* Release 6.4, GmbH, June 2009.

[11] MATLAB 7.12.0 (R2011a), A software by Mathworks Inc.

[12] dSPACE *Real-Time Interface (RTI and RTI-MP): Implementation guide*, Release 6.6, GmbH, May 2010.

[13] dSPACE *Conrol Desk: Experiment guide*, Release 6.6, GmbH, May 2010.

[14] J. W. Tester, E. M. Drake, M. J. Driscoll, M. W. Golay and W. A. Peters, *Sustainable Energy: Choosing Among Options,*, The MIT Press, Cambridge, Massachussets, 2005.

[15] B. Wu, Y. Lang, N. Zargari and S. Kouro, *Power Conversion and Control of Wind Energy Systems,* IEEE Press, John Wiley and Sons Inc., 2011.

[16] O. Anaya-Lara, N. Jenkins, J. Ekanayake, P. Cartwright and M. Hughes, *Wind Energy Generation: Modelling and Control,* John Wiley and Sons Ltd, West Sussex, England, 2009.

[17] Q. Zeng, L. Chang and R. Shao, "Fuzzy logic based maximum power point tracking strategy for PMSG variable-speed wind turbine generation systems," Proccedings of IEEE Canadian Conference on Electrical and Computer Engineering, Fredericton, NB, May 2008.

[18] F. Valenciga and P. F. Puleston, "High-order sliding control for a wind energy conversion system based on a permanent magnet synchronous generator," *IEEE Transactions on Energy Conversion,* vol.23, no. 3, pp. 860-867, Sept. 2008.

[19] D. Yu and S. Yuvarajan, "Load sharing in a hybrid power system with PV panels and a PEM fuel cell," Proceedings of IEEE Applied Power Electronics Conference, Mar. 2006.

[20] T. Esram and P. Chapman, "Comparison of photovoltaic array maximum power point tracking techniques," *IEEE Transactions on Energy Conversion,* vol.22, no. 2, pp. 439-449, June 2007.

[21] V. Salas, E. Olias, A. Barrado and A. Lazaro, "Review of maximum power tracking algorithms for standalone photovoltaic systems," Solar Energy Materials and Solar Cells, vol. 90, pp. 1555-1578, Jan. 2006.

[22] S. Yuvarajan and Yinying Kuai, "An improved voltage-based maximum power point tracking method for photovoltaic panels," Proceedings of Power Systems World Conference, Baltimore, October 2005.

[23] S. Yuvarajan, D. Yu and S. Xu, "A novel power converter for photovoltaic applications," Journal of Power Sources, vol. 135, no. 1-2, pp. 327-331, Sept. 2004.

[24] N. A. Orlando, M. Liserre, V. G. Monopoli, R. A. Mastromauro and A. Dell'Aquila, "Comparison of power converter topologies for permanent magnet small wind turbine system," Proceedings of IEEE International Symposium on Industrial Electronics, 2008.

[25] Ned Mohan, *First Course on Power Electronics*, MNPERE, Minneapolis, 2009.

[26] H. Geng, G. Yeng, D. Xu and B. Wu, "Unified power control for PMSG-based WECS operating under different grid conditions," *IEEE Transactions on Energy Conversion*, vol.26, no. 3, pp. 822-830, Sept. 2011.

[27] M. H. Rashid, *Power Electronics: Circuits, Devices and Applications, 3rd Edition*, Prentice Hall, 2003.

[28] R. Ridley, "Analyzing the SEPIC Converter," published by Power Systems Design Europe, Nov. 2006, available at http://www.switchingpowermagazine.com/downloads/Sepic%20Analysis.pdf

[29] N. Mohan, T. M. Undeland and W. P. Robbins, *Power Electronics: Converters, Applications and Design, 3rd Edition*, John Wiley and Sons, 2002.

[30] PSIM, A Software by Powersim Technologies, Professional Version 9.0.

[31] MATLAB Simpowersystems, published by Mathworks Inc.

[32] M. Chinchilla, S. Arnaltes and J. C. Burgos, "Control of permanent-magnet generators appiled to variable-speed wind-energy systems connected to the grid," *IEEE Trans.Energy Conversion*,vol. 21, no. 1, pp. 130-135, March 2006.

[33] L. Chang, “Wind energy conversion systems,” IEEE Canadian Review, No. 40, p.2, Spring 2002.

[34] T. Ackermann, *Wind Power in power Systems*, John Wiley and Sons, West Sussex, England, 2005.

[35] S. Muller, M. Deicke and R. W. De Doncker, “Doubly fed induction generator systems,” IEEE Industry Applications Magazine, pp. 26-33, May-June 2002.

[36] Z. Q. Zhu and D. Howe, “Electrical Machines and Drives for Electric, Hybrid and Fuel Cell Vehicles,” Proceedings of the IEEE, vol. 95, no. 4, pp. 746-765, April 2007.

[37] A. Aleksashkin and A. Mikkola, “Literature review on permanent magnet generators design and dynamic behaviour,” Research report 77, Department of Mechanical Engineering, Lappeenranta University of Technology, Lappeenranta, Finland, 2008.

[38] D. Svechkarenko, “Simulations and control of direct driven permanent magnet synchronous generator,” Project report, Department of electrical Engineering, Royal Institute of Technology, Sweden, 2005.

[39] X. Wang, S. Yuvarajan and L. Fan, “MPPT control for a PMSG-based grid-tied wind generation system,” Proceedings of IEEE North American Power Symposium, Sept. 2010.

[40] S. Yuvarajan and Juline Shoeb, “A fast and accurate maximum power point tracker for PV systems,” Proceedings of IEEE Applied Power Electronics Conference , Feb. 2008.

[41] A. Mondal and S. Yuvarajan, “MPPT scheme for small scale photovoltaic systems using dSPACE,” Proceedings of IEEE Green Technoogies Conference, Tulsa, OK, April 2012.

APPENDIX. LIST OF PUBLICATIONS

1. A. Mondal and S. Yuvarajan, "MPPT Scheme for Small Scale Photovoltaic Systems using dSPACE," Proceedings of IEEE Green Technologies Conference, Tulsa, OK, April 2012.
2. A. Mondal and S. Yuvarajan, "A Permanent Magnet Synchronous Generator based Wind Energy System assisted by Solar Power," accepted for presentation at IEEE Symposium on Power Electronics and Machines in Wind Applications (PEMWA), Denver, CO, July 2012.